

Spatial distribution of the electronic wave function of the shallow boron acceptor in 4H- and 6H-SiC

A. van Duijn-Arnold, J. Mol, R. Verberk, and J. Schmidt

Huygens Laboratory, Leiden University, P.O. Box 9504, 2300 RA Leiden, The Netherlands

E. N. Mokhov and P. G. Baranov

A. F. Ioffe Physico-Technical Institute, Politechnicheskaya 26, 194021 St. Petersburg, Russia

(Received 27 April 1999; revised manuscript received 22 June 1999)

A high-frequency (95 GHz) pulsed electron paramagnetic resonance and electron-nuclear-double-resonance study has been carried out on the shallow boron acceptor in ^{13}C -enriched 4H-SiC and 6H-SiC. From the hyperfine interaction of the unpaired electron spin with the ^{13}C ($I=1/2$) nuclei the spatial distribution of the electronic wave function has been established. It is found that there are subtle differences in the degree of localization of this wave function between the different sites (two quasicubic and one hexagonal) in the two polytypes 4H-SiC and 6H-SiC, though only for the two quasicubic sites a complete study of the wave function could be made. In particular it is found that the spatial distribution is highly anisotropic. This anisotropy can be rationalized by considering the anisotropy of the hole mass, i.e., by assuming that effective-mass theory is (partly) valid in describing the remote part of the spatial distribution of the electronic wave function. [S0163-1829(99)16135-6]

I. INTRODUCTION

One of the intriguing problems in semiconductor physics is the nature of shallow impurities in the host-crystal lattice. The most critical test of the theoretical models describing the electronic wave function of the shallow donors and acceptors is provided by the hyperfine interaction of the unpaired electron spin with the surrounding nuclear spins, obtained from electron-nuclear-double-resonance (ENDOR) spectroscopy. This ENDOR technique, developed by Feher,¹ has been successfully applied to the three donor impurities P, As, and Sb in Si.¹⁻³ In contrast, all attempts to observe ENDOR from group-III acceptors (B, Al, Ga) in Si have been unsuccessful, although electron paramagnetic resonance (EPR) signals could be observed after applying uniaxial stress which removes the degeneracy of the valence band.⁴ The reason for the failure to observe ENDOR of acceptors in Si is related to the presence of random stress in the crystal which, in combination with the degeneracy of the valence band, leads to variations in the g -tensor values and to a broadening of the ENDOR lines.

In this paper we present a determination of the spatial delocalization of the electronic wave function of an acceptor in a semiconductor. The system studied is the B acceptor in SiC. Silicon carbide has a crystal structure which is very close to that of silicon. Especially cubic SiC (3C-SiC), which has a zinc-blende structure, is very similar. The structure of other polytypes is different, and some of them are hexagonal. It is known that the most important acceptor impurities in SiC are B, Al, and Ga, as in Si. These group-III elements can be introduced during growth or afterwards by diffusion or implantation and have been studied using Hall effect, optical spectroscopy,⁵ and deep-level transient spectroscopy.^{6,7} Shallow acceptors introduced in SiC by the group-III impurities have also been studied using EPR,⁸⁻¹³ optically detected magnetic resonance (ODMR),¹³⁻¹⁶ high-frequency pulsed EPR and ENDOR at 95 GHz,¹⁷ and by ENDOR at conven-

tional frequencies.^{18,19} The activation energies for shallow boron (sB) acceptors were estimated to be between 0.22 eV and 0.35 eV.⁴ More recently it was found by Evwaraye *et al.*²⁰ that the activation energy is $E_v+0.27$ eV for the hexagonal site (hex) and $E_v+0.31$ eV and $E_v+0.38$ eV for the quasicubic sites k_1 and k_2 , respectively. According to Ref. 21, the incorporation of Al in 6H-SiC introduces shallow acceptor levels at $E_v+0.239$ eV for the hexagonal site (hex) and $E_v+0.248$ eV for the quasicubic sites (k_1, k_2). Similarly, Ga introduces shallow acceptor levels at $E_v+0.317$ eV (hex) and $E_v+0.333$ eV (k_1, k_2).²¹

There is a large difference in the properties of group-III shallow acceptors in SiC and Si. In Si all group-III shallow acceptors show effective-mass-like behavior with the B acceptor as the shallowest level. In SiC, the energy level of sB is roughly situated between that for shallow Al (sAl) and for shallow Ga (sGa). However, it appears, that the electronic structure of the sB acceptor is strikingly different from that of the sAl and sGa acceptor. The resonance conditions of the unpaired spin related to the sAl and sGa acceptors reflect the properties of the uppermost Γ_9 valence-band hole, and indicate an effective-mass-like character of these acceptors, but with a reduced orbital-momentum contribution resulting from the localization. In contrast, the EPR spectrum of the sB acceptor shows that the contribution of the orbital angular momentum is almost negligible ($g\sim 2$), and EPR signals of sB could be observed in 3C-SiC without any uniaxial stress applied to the crystal. In contrast sAl and sGa signals have not been observed in 3C-SiC.

The difference in behavior of sB on the one hand, and sAl and sGa on the other hand, was explained by considering the difference in atomic radii.^{12,13,17} It was proposed that B, which substitutes for Si but which has an atomic radius smaller than Si, occupies an off-center position owing to chemical rebonding, i.e., it relaxes away from the neighboring C along the B-C bond. Indeed a high-frequency (95

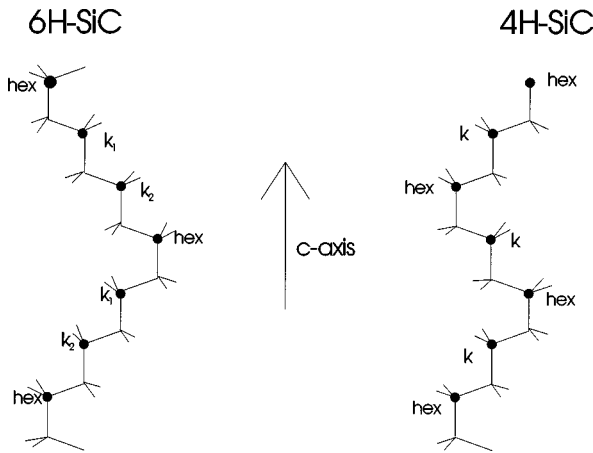


FIG. 1. A schematic representation of the difference between the $4H$ - and $6H$ -SiC crystal structures. The SiC crystal is built up of tetrahedrons, with four bonds for every atom. Two of the bonds lie in the plane of the figure and parallel to the direction of the c axis a staircase pattern is formed. For $6H$ -SiC this pattern gives rise to three inequivalent sites k_1 , k_2 and hex, for $4H$ -SiC the staircase is shorter and there are only two sites, k and hex.

GHz) EPR and ENDOR study on sB in $6H$ -SiC, carried out at liquid-helium temperatures, revealed that there is a relaxation of the neighboring carbon atom and the boron atom away from each other.¹⁷ This study also revealed that B is neutral, and that it carries no direct spin density. The main spin density (about 30%) is located on the dangling bond p_z orbital of one of the neighboring carbon atoms along the C-B connection line. In contrast to the behavior of the sB acceptor, Al and Ga atoms substituting for Si are expected to occupy on-center positions. As the local symmetry is conserved this could explain the effective-mass-like-behavior observed for the sAl and sGa acceptors.

The aim of the present study is to reveal the spatial distribution of the electronic wave function of the sB acceptor in different sites (quasicubic and hexagonal) in the two polytypes $4H$ -SiC and $6H$ -SiC. Fukumoto, using the first-principles pseudopotential method,²² calculated that the unpaired electron connected to the sB acceptor center in $3C$ -SiC resides almost entirely on the C atoms. Thus we have performed a 95-GHz ENDOR study on the ^{13}C ($I = \frac{1}{2}$) nuclear spins in ^{13}C -enriched SiC crystals to obtain the hyperfine (hf) interaction with the unpaired spin density. From the results it appears that, although the EPR properties of sB in $4H$ -SiC and $6H$ -SiC are very similar, a difference in behavior can be observed in the ENDOR data. In particular it can be seen that for the k_2 site in $6H$ -SiC the electronic wave function is slightly more localized than for the k_1 site in $6H$ -SiC and the k site in $4H$ -SiC. Unfortunately a similar detailed analysis of the hexagonal site was not possible due to a congestion of lines in the ENDOR spectrum. Nevertheless a tentative spatial distribution of the electronic wave function for this site is proposed. [For a definition of the quasicubic (qc) sites and hexagonal (hex) site in $4H$ -SiC and $6H$ -SiC, see Fig. 1]. Our conclusion agrees with the finding of Evwaraye *et al.*²⁰ that the binding energies for the three sites of the sB acceptor in $6H$ -SiC differ.

A remarkable result is that the spatial delocalization of the unpaired spin density of the qc-site-related sB acceptor is

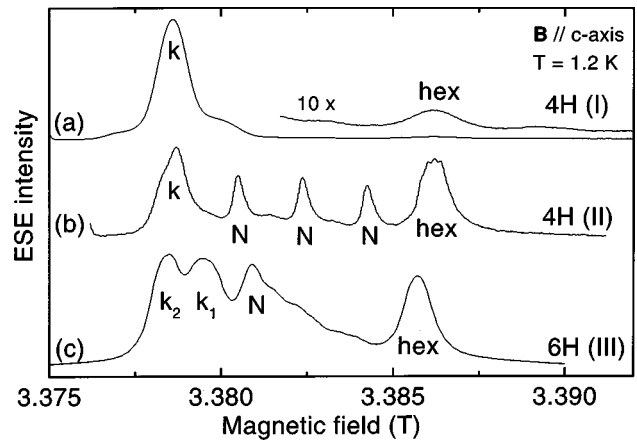


FIG. 2. (a) The EPR spectrum at 95 GHz with $\mathbf{B} \parallel \mathbf{c}$ for the sB acceptor in $4H$ -SiC (sample I). The spectrum consists of two lines; one is related to a B atom on the k site, and one to a B atom on the hex site. The shoulders are attributed to the hf interaction with the nearest-neighbor ^{13}C nuclei. (b) A similar EPR spectrum obtained on sample II. In addition to the sB lines, three lines are observed of the shallow N donor on the k site in $4H$ -SiC. This triplet is attributed to the hf interaction with the ^{14}N nuclear spin ($I = 1$). (c) The EPR spectrum at 95 GHz with $\mathbf{B} \parallel \mathbf{c}$ for the sB acceptor in $6H$ -SiC. In addition to the EPR lines of the sB acceptor on the k_1 , k_2 , and hex positions, a signal is observed that is attributed to the shallow N donor. All spectra are recorded at 1.2 K.

highly anisotropic. This spatial distribution agrees very well with theoretical predictions of Petrenko *et al.*²³ Interestingly this anisotropy can be rationalized by considering the anisotropy of the effective mass of the hole. So it seems that the properties of the remote part of the sB acceptor wave function can still be explained (partly) by effective-mass theory, although the orbital angular momentum of the hole is quenched as a result of the lattice distortion.

II. EXPERIMENT

The experiments were performed on the following three different samples. The first (sample I) is a free-standing $4H$ -SiC epitaxial layer (with removed substrate), grown by the sublimation sandwich method²⁴ in vacuum at temperatures between 1700 and 1750 °C. It is ^{13}C enriched (30%), contains boron in natural abundance and is p type. Boron was introduced during growth because it was present as a trace impurity in the material used for the ^{13}C source. As such no N was present in this sample. The second $4H$ -SiC sample (II) is from Cree Company, it is also p type, and ^{11}B was diffused at a temperature of about 2000 °C. The third $6H$ -SiC sample (III) is also ^{13}C enriched and p type. It is a free-standing epitaxial layer (with removed substrate), grown in the same way as sample I, with ^{11}B diffused in at temperatures of about 2000 °C. It should be mentioned that the central part of samples II and III is not compensated by B. It is still n type, and leads to the presence of N-related lines in the EPR spectrum. Typical sample dimensions are $0.2 \times 0.4 \times 0.2 \text{ mm}^3$.

The experiments were performed at 1.2 K on a home-built, pulsed EPR/ENDOR spectrometer operating at a microwave frequency of 95 GHz. A detailed description of the setup is given elsewhere.^{25,26} The main advantage of this

TABLE I. The g -tensor principal values of the sB acceptor and the hf interaction with the nearest-neighbor carbon atom for the hexagonal site as well as the quasicubic site, in the case of $4H$ -SiC (this work, Refs. 9 and 32) and of a $6H$ -SiC crystal (Ref. 17). All g values have been calculated relative to g_z of the hexagonal site, assuming it to have a value of 2.002 00. The temperature in Ref. 9 was 3.4 K and the microwave frequency was 74.1 GHz. The temperature in Ref. 32 was 4.2 K, and the microwave frequency was 142 GHz.

		g_x	g_y	g_z	$a(C)$ ($\times 10^{-4}$ T)	$b(C)$ ($\times 10^{-4}$ T)
$4H$	k	2.0069(1)	2.0056(1)	2.0020(1)	39(1)	12.5(6)
	k (Ref. 9)	2.0028(5)	2.0059(5)	2.0064(5)	32(1)	7.3(5)
	k (Ref. 32)	2.0069(2)	2.0059(3)	2.0025(2)		
	hex	2.0066(1)	2.0066(1)	2.0020	39(1)	12.5(5)
	hex (Ref. 9)	2.0070(5)	2.0070(5)	2.0018(5)	32(1)	7.3(5)
	hex (Ref. 32)	2.0070(2)	2.0070(2)	2.0019(2)		
$6H$	k_1 (Ref. 17)	2.00623(5)	2.00605(5)	2.00226(5)	40.8(5)	10.8(5)
	k_2 (Ref. 17)	2.00592(5)	2.00675(5)	22.00251(5)	40.8(5)	10.8(5)
	hex (Ref. 17)	2.0069(5)	2.0069(5)	2.00200	40.8(5)	10.8(5)

spectrometer is the high resolution both in the EPR and ENDOR spectra. Moreover, owing to the split-coil configuration of the superconducting magnet, it is possible to perform a complete orientational study. The pulsed electron-spin-echo-detected EPR spectra were measured by monitoring the electron spin echo intensity in a two-pulse echo experiment as a function of the magnetic field. In the pulsed ENDOR experiment a Mims-type pulse sequence was used,²⁷ consisting of three $\pi/2$ microwave pulses with separations τ and T between the first and the second, and second and third, pulses, respectively. Typical values for τ and T are 250 ns and 1 ms, respectively. As a result of this pulse sequence a stimulated echo (SE) is created at a time τ after the last pulse. During the time T , which is much longer than the phase memory time T_M , a radiofrequency (rf) pulse is applied which induces a change in the intensity of the SE when this rf pulse is resonant with a nuclear transition. The ENDOR spectra are obtained by monitoring the SE intensity as a function of the frequency of the rf field.

III. RESULTS AND ANALYSIS

The EPR and ENDOR data to be discussed in this section can be described by a spin Hamiltonian of the form.

$$H = \mu_B \vec{S} \cdot \vec{g} \cdot \vec{B} + (\vec{S} \cdot \vec{A}_B - \gamma_B \vec{B}) \cdot \vec{I}_B + \vec{I}_B \cdot \vec{P}_B \cdot \vec{I}_B + \sum_i (\vec{S} \cdot \vec{A}_X^i - \gamma_X \vec{B}) \cdot \vec{I}_X, \quad (1)$$

where X represents Si or C, \vec{A}_B and \vec{A}_X^i represent the hyperfine tensors of the ^{11}B ($I = \frac{3}{2}$), ^{13}C ($I = \frac{1}{2}$), and ^{29}Si ($I = \frac{1}{2}$) nuclear spins, \vec{P}_B the quadrupole tensor of the $^{11}\text{B}/^{10}\text{B}$ spins, and γ_B and γ_X the gyromagnetic ratios for the B, C, and Si nuclei. We can write for the hyperfine tensor $A_{zz} = a + 2b$, $A_{yy} = a - b - b'$, and $A_{xx} = a - b + b'$. For the quadrupole interaction we can write, assuming axial symmetry, $P_B(I_z^2 - 1/3 I^2)$ with $P_B = 3/2 P_{zz} = 3q$ and $P_{xx} = P_{yy} = -q$.

A. EPR spectra

Figure 2 shows three 95-GHz EPR spectra of the sB acceptor in SiC with $\mathbf{B} \parallel c$ axis. The upper spectrum is obtained on sample I ($4H$ -SiC) and consists of two lines; one is related to a B atom on a quasicubic position (k) in the crystal, the other is related to a B atom on a hexagonal position (hex). The latter line is only visible after magnifying the spectrum by a factor 10. The weakness of the hex signal is probably caused by the position of the Fermi level. The weak satellites in the magnified spectrum are caused by the hyperfine (hf) interaction with the nearest-neighbor ^{13}C nucleus. The middle spectrum was measured on sample II ($4H$ -SiC). Here, in addition to the two EPR signals of the sB acceptor, the signal of the k -site N donor, present in the central, uncompensated part of the sample, is observed, with a hf splitting in three components characteristic of $4H$ -SiC and caused by the ^{14}N ($I = 1$) nuclear spin. We remark that, owing to the small linewidth of the sB signals and the fact that this sample is not ^{13}C enriched, the hf interaction with the B nuclear spin is visible in this spectrum on the sB line related to the hex site. The lowest spectrum is obtained under similar conditions on sample III (^{11}B -doped $6H$ -Si ^{13}C). The three lines marked with k_1 , k_2 , and hex correspond to the two qc sites and the hex site of the sB acceptor. We remark that the assignment of the EPR lines to the k_1 or k_2 site is reversed with respect to earlier publications.^{9,17} This reassignment is based on the ENDOR data to be presented in this paper (see Sec. II B 2). The broad line marked with N originates from the qc and hex site N donors, present in the central part of this sample, which is not totally compensated with ^{11}B .

To find the g tensor of the sB center in $4H$ -SiC, we made a study of the orientational dependence of the EPR spectrum in two planes. The first dependence was measured in the $(11\bar{2}0)$ plane, in which the magnetic field is turned from $\mathbf{B} \parallel c$ axis toward the plane perpendicular to \mathbf{c} ($\theta = 0^\circ \rightarrow 90^\circ$, $\varphi = 0^\circ$, with θ the angle between the c axis and the magnetic field). The second dependence was measured in the plane perpendicular to the c axis ($\theta = 90^\circ$ and $\varphi = 0^\circ$

$\rightarrow 90^\circ$). For the orientation $\theta = 90^\circ$ and $\varphi = 0^\circ$, the magnetic field lies along the projection of a C-Si bond in the plane perpendicular to the c axis. In analogy with the case of the sB acceptor in 6H-SiC,¹⁷ it is found that the principle axes g_z , g_x , and g_y for the k site are directed with $g_z \parallel$ B-main C bond (70° to c), g_x perpendicular to g_z in the plane spanned by the c axis and the B-main C bond and the g_y axis perpendicular to both, in the plane perpendicular to the c axis. For the hex site, the g_z axis is found to be parallel to the c axis, and the g_x axis lies in the same plane as for the k site, again perpendicular to the g_z axis. The g_y axis makes an angle of 90° with both. In Table I the principle g values are presented and it is seen that they are also almost the same as for sB in 6H-SiC. The largest relative difference is found in g_x . As the deviation of the g value from g_e scales with the energy difference between two levels, it is sensitive to changes in the surroundings. The g value that differs most from g_e will thus relatively be most sensitive to changes.

The ^{13}C hf splitting observed in the EPR spectra and related to the C atom carrying the main spin density exhibits axial symmetry with the symmetry axis parallel to the g_z axis of the site. The fit values to the experimental data of the ^{13}C hf interactions are also collected in Table I, where we used the definitions $A_{zz} = a + 2b$ and $A_{xx} = A_{yy} = a - b$. A comparison with similar observations in 6H-SiC shows that the isotropic parameters, a are the same within experimental error, but that the anisotropic parameters b are slightly different. In analogy with Ref. 17, we conclude that a and b are both positive as based on the orientational dependence and the mere size of the hf interaction.

At certain orientations shoulders can be seen on the sB EPR lines. These lines were also reported in previous papers^{8,9,17} and attributed to the hf interaction with ^{29}Si ($I = \frac{1}{2}$) nuclei of the first Si shell, i.e., the three Si next to the carbon carrying the main spin density. The hf interaction of these lines was reported to be virtually isotropic ($b < 1 \times 10^{-4}$ T), with an isotropic hf constant $a = 10 \times 10^{-4}$ T.

B. ENDOR

Figure 3 shows an overview of the total ENDOR spectrum as measured on the 4H-Si ^{13}C sample with a natural abundance of B (sample I) with $\mathbf{B} \parallel c$. The figure is a nice example of the spectral resolution that can be obtained at 95 GHz. The orientational dependence of the ENDOR spectra is obtained by tuning the magnetic field to the EPR line of the site studied. In the following we will concentrate on the different parts of the spectrum.

1. ENDOR of ^{11}B and ^{10}B

From the orientational dependence of the boron ENDOR spectra, it was found that there is a striking similarity between the hexagonal and qc sites in 4H-SiC and 6H-SiC. The tensors are axially symmetric, with their axes of symmetry along the g_z axis of a specific subsite and with similar principal values. The results are summarized in Table II. The measurements on ^{11}B ($I = \frac{3}{2}$) and ^{10}B ($I = 3$) allowed us to check whether the different isotopic masses had an effect on the hf data. However, we found that the hf data for the two isotopes are simply related by taking account of the different gyromagnetic ratios, the ratio of the quadrupole moments

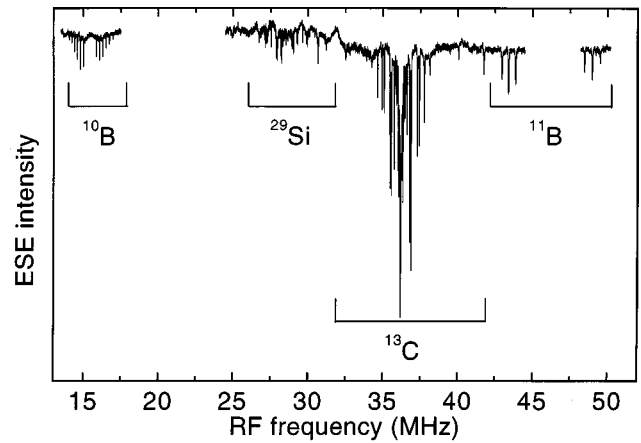


FIG. 3. The ENDOR spectrum as measured on the EPR line of the k site in 4H-SiC for $\mathbf{B} \parallel c$ at 1.2 K. It shows the clear separation of the ENDOR lines belonging to the different isotopes and nuclei. As the sample is ^{13}C enriched, the ENDOR lines for this isotope are very intense. Only for the outer ^{13}C ENDOR lines there is some overlap with the ^{29}Si and ^{11}B lines.

and a spin factor $2I(2I-1)$. The signs of a , b , and q in Table II were determined in the same way as described in Ref. 17. The relative signs of $A = a + 2b(3 \cos^2 \theta)$ and $Q = q(3 \cos^2 \theta)$ were determined using field-tagged ENDOR, from which it followed that the hf interaction A and the quadrupole interaction Q have the same sign for both sites in 4H-SiC. From the fit of the orientational dependence it followed that a and b have an opposite sign, which means that either $a < 0$ and $b > 0$, $q > 0$ or $a > 0$ and $b < 0$, $q < 0$. The absolute sign is determined from theory, which shows that q is expected to be positive (see discussion).

2. ENDOR of ^{13}C

Figure 4 shows part of the ^{13}C ENDOR spectra of the sB k_1 and k_2 site in 6H-Si ^{13}C : ^{11}B (sample III) and the k site in 4H-Si ^{13}C (sample I). The first thing to note is that the k_1 spectrum in 6H-SiC is the same, except intensities, as that of the k site in 4H-SiC. This is the case for all measured orientations, which leads us to the conclusion that these two centers have the same position and thus the same surrounding in the crystal. We thus assign the corresponding EPR line to the k_1 site, as this site is situated at a similar crystal position as the k site in 4H-SiC. Moreover, these two sites have the same environment in the two layers perpendicular to the c axis above and below the B center, which we used in the assignment of the ENDOR lines. This conclusion is opposite to what has been published previously.¹⁷ This earlier assignment was based on the anisotropy of the g tensor. The EPR line with the smallest g -tensor anisotropy was assigned to the site closest to the hex site, as the g tensor of the hexagonal site is axial. Also, the argument of the relaxation time seemed to point to this conclusion, because, when assuming an isotropic spin-density distribution around the B center the sites sharing the same carbon atom should have the same relaxation time. As it will turn out, the spin density distribution is not isotropic at all, and consequently this argument is not valid. The second thing to note is that the spectrum of k_2 contains less lines around the carbon nuclear

TABLE II. The hyperfine parameters a , b , and q for ^{11}B as found in this study and in Refs. 9 and 32 on the sB acceptor in $4H$ -SiC. In addition, the same parameters are listed for sB in $6H$ -SiC. The parameters a , b , and q are related to the parameters A and Q as follows: $A_{\parallel} = a + 2b$, $A_{\perp} = a - b$, and $Q_{zz} = 2q$. The temperature in Ref. 32 was 4.2 K, and the microwave frequency was 9.5 GHz.

		$a(^{11}\text{B})$ MHz	$b(^{11}\text{B})$ MHz	$q(^{11}\text{B})$ MHz
$4H$	k	-3.4(2)	2.9(1)	242(31)
	k (Ref. 9)	1.3(2)	0.18(1)	
	k (Ref. 32)	$\pm 3.365(10)$	$\pm 2.888(10)$	$\pm 257(10)$
	hex	-0.85(9)	2.55(9)	253(8)
	hex (Ref. 9)	1.5(2)	0.13(1)	
	hex (Ref. 32)	$\mp 0.412(10)$	$\pm 2.915(10)$	$\pm 255(10)$
$6H$	k (Ref. 17)	-3.72(5)	3.06(5)	255(5)
	k (Ref. 17)	-2.99(5)	2.89(5)	250(5)
	hex (Ref. 17)	-0.97(5)	2.91(5)	242(5)

Zeeman frequency than that of k_1 which, combined with the fact that we found one more line at 45 MHz for k_2 , suggests that for k_2 the spin density is more localized than for k_1 . Above the k_2 ENDOR spectrum, a rescaled part of the k_1 spectrum is shown for comparison, from which it can be seen that the ENDOR lines belonging to the k_1 site are also weakly present in the k_2 ENDOR spectrum. Only the two strong lines at 37.7 and 38.65 MHz belong to the k_2 site. Very weakly, the strongest k_2 lines can also be seen in the k_1 spectrum. This ‘‘crosstalk’’ is the result of the small overlap of the EPR lines of the k_1 and k_2 sites in $6H$ -SiC.

To illustrate the complexity of the assignment of the ENDOR lines, we show in Fig. 5(a) the orientational dependence of the inner part of the ^{13}C ENDOR spectrum of the k_1 site of sB in $6H$ -SiC where \mathbf{B} is varied in the plane perpendicular to the c axis from $\mathbf{B} \parallel \varphi = 0^\circ$ to $\mathbf{B} \parallel \varphi = 90^\circ$. Figure 5(b)

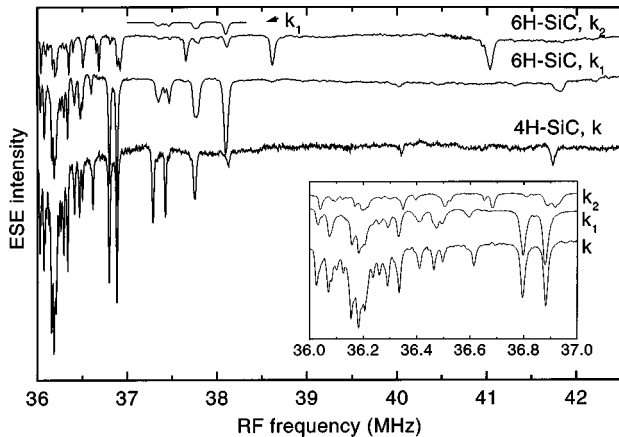


FIG. 4. The ^{13}C ENDOR lines with $\mathbf{B} \parallel \mathbf{c}$ and at 1.2 K for the different sites in $6H$ -SiC (k_1 and k_2) and $4H$ -SiC (k). As can be seen, the spectrum of k is very similar to that of k_1 . A rescaled part of the spectrum of k_1 is shown above the spectrum of k_2 in the region between 37 and 38.3 MHz. From the intensity comparison it is clear that the lines that show up in both spectra belong to k_1 . The two lines at 38.7 and 37.7 MHz belong to k_2 . These two lines can also be seen weakly in the spectrum of k_1 . In the inset a blowup of the spectrum around the ^{13}C nuclear Zeeman frequency is shown.

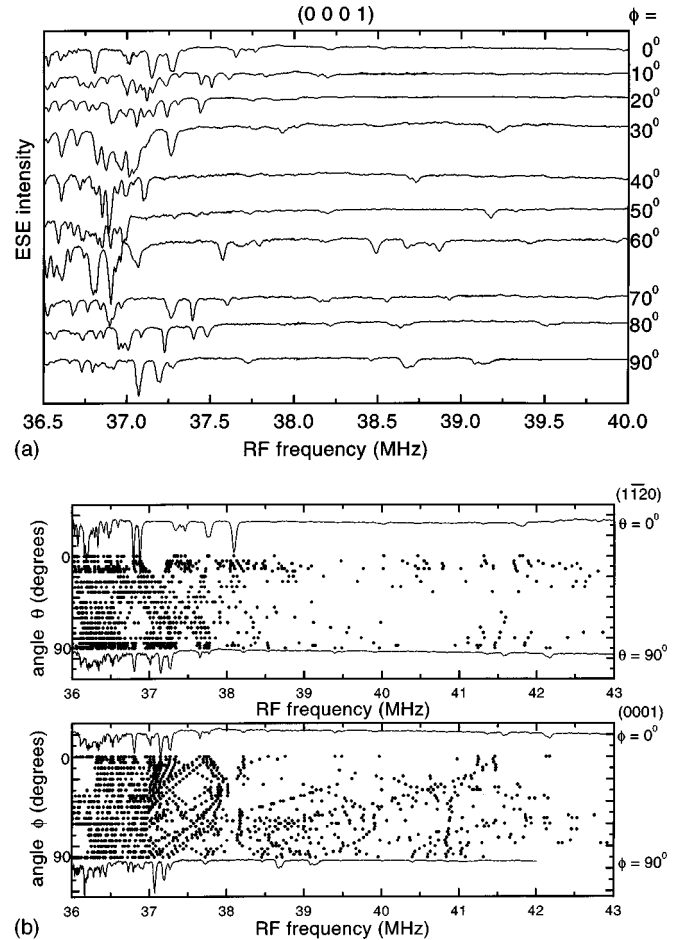


FIG. 5. (a) The orientational dependence of the ENDOR lines of the k_1 site of the sB center in $6H$ -SiC in the plane perpendicular to the c axis from $\mathbf{B} \parallel \varphi = 0^\circ$ to $\mathbf{B} \parallel \varphi = 90^\circ$ at 1.2 K. As can be seen, the ENDOR lines are very anisotropic. (b) The orientational dependence of the ENDOR lines as measured on the k_1 site EPR line of the sB center in the $(11\bar{2}0)$ and (0001) planes at 1.2 K. The points represent the ENDOR lines as measured for the respective orientations of the magnetic field. As can be seen, the lines are very anisotropic, and the largest hf interaction is about 12 MHz.

TABLE III. The positions of the nuclei in the k_1 site in $6H$ -SiC, their tensor directions, hf interactions, distance to the B center, and coefficients α^2 , β^2 , and η^2 of the electronic wave function. For the nuclei of groups II, III and IV with a question mark as superscript, the determination of the second Euler angle is not very precise. The tensors of the groups VIII and XI are oriented towards the center of gravity of the p_z orbital on the main C (I), as for these nuclei there is an appreciable contribution from the dipole-dipole interaction to the anisotropic hf interaction. The first pair of nuclei of group XI has not been found in the orientational dependence. The total spin density found when summing over all nuclei is 105%, even though not all lines have been assigned. Nevertheless η^2 has been normalized to 100%. The atom positions with the same symbols as superscripts can in principle be interchanged. This does not affect the spin-density distribution appreciably.

k_1	Atom position	Euler angles (α, β, γ) in degrees	a (MHz)	b (MHz)	b' (MHz)	Distance to the B nucleus (Å)	s to p ratio ($\alpha^2:\beta^2$)	Percentage of total (η^2)
I	c_0y_0	(0,70.5,0)	114 ± 1	30 ± 1		1.887	9.7:90.3	29.5
II	$c_0y_{\pm 1}^?$	(17.5,72,0)	14.2 ± 0.1	3.8 ± 0.1	-0.5 ± 0.1	4.75	9.6:90.4	3.7
	$c_{+1}y_{\pm 1}^?$	($\pm 60, 70.5, 0$)	14.70 ± 0.02	-2.93 ± 0.01	-6.17 ± 0.05	4.41		
III	c_0y_0	(0,80.5,0)	12.75 ± 0.07	3.11 ± 0.08	1.34 ± 0.08	7.14	10.4:89.6	3.1
	$c_{+1}y_0$	(0,55,0)	7.88 ± 0.08	3.97 ± 0.12	-0.6 ± 0.1	6.20	5.3:94.7	3.7
IV	$c_0y_{\pm 2}$	($\pm 17, 70.5, 0$)	7.71 ± 0.07	5.3 ± 0.1	1.43 ± 0.09	7.78	4.0:96.0	4.9
	$c_{+1}y_{\pm 2}$	($\pm 77, 70.5, 0$)	7.71 ± 0.07	5.3 ± 0.1	1.43 ± 0.09	6.92	4.0:96.0	4.9
	$c_{+2}y_0$	(0,45,0)	5.37 ± 0.04	2.50 ± 0.06	1.59 ± 0.08	7.78	5.7:94.3	2.3
V	$c_{+1}y_{\pm 1}$	($\pm 3, 67.5, 0$)	5.38 ± 0.08	3.26 ± 0.09	-1.0 ± 0.1	8.74	4.5:95.5	3.0
	$c_0y_{\pm 1}$	(0,80.5,0)	6.94 ± 0.07	1.60 ± 0.05	2.20 ± 0.09	9.92	11.0:89.0	1.6
	$c_{+2}y_{\pm 1}$	($\pm 60, 70.5, 0$)	5.76 ± 0.09	2.93 ± 0.09	-0.12 ± 0.02	8.56	5.3:94.7	2.7
VI	$c_{+1}y_{\pm 3+}$	($\pm 60, 70.5, 0$)	4.67 ± 0.05	0.86 ± 0.08	-0.59 ± 0.07	9.78	13.4:86.6	0.9
VII	$c_0y_{\pm 3}$	(0,77.5,0)	3.67 ± 0.03	1.99 ± 0.03	0.34 ± 0.05	10.85	5.0:95.0	1.8
	$c_{+2}y_{\pm 3}^{+, \#}$	($\pm 60, 77.5, 0$)	3.67 ± 0.03	1.99 ± 0.03	0.34 ± 0.05	9.61	5.0:95.0	1.8
VIII	$c_0y_{\pm 1}$	($\pm 37, 84, 0$)	2.03 ± 0.04	0.84 ± 0.04		1.887	6.4:93.6	0.8
	$c_{-1}y_0$	(0,32,0)	2.03 ± 0.04	0.84 ± 0.04		1.89	6.4:93.6	0.8
IX	$c_0y_{\pm 4}^{\#}$	($\pm 25, 85, 0$)	2.01 ± 0.02	0.68 ± 0.02		9.44	7.8:92.2	0.7
X	$c_{+2}y_{\pm 1}$	(0,107.5,0)	1.79 ± 0.04	1.28 ± 0.04	-0.92 ± 0.08	5.94	3.8:96.2	1.2
	$c_0y_{\pm 3}^{\#}$	($\pm 60, 70.5, 0$)	1.79 ± 0.04	1.28 ± 0.04	-0.92 ± 0.08	6.44	3.8:96.2	1.2
XI	$c_0y_{\pm 2}$	($\pm 76.7, 85, 0$)	~ 0.5	~ 0.2		3.61		
	$c_{-1}y_{\pm 1}$	($\pm 40, 135, 0$)	0.53 ± 0.01	-0.14 ± 0.02	0.58 ± 0.04	3.61	9.7:90.3	0.1
	$c_{+1}y_0$	(0,22,0)	1.72 ± 0.02	-0.66 ± 0.02	-0.65 ± 0.03	3.61	6.9:93.1	0.6
XII	$c_{+1}y_0$	(0,70,0)	1.08 ± 0.01	0.52 ± 0.01	0.57 ± 0.02	11.13	5.6:94.4	0.5
	$c_{+2}y_0$	(0,41,0)	0.74 ± 0.02	-0.11 ± 0.02	0.73 ± 0.03	10.55	16.1:83.9	0.1

TABLE III. (Continued).

k_1	Atom position	Euler angles (α, β, γ) in degrees	a (MHz)	b (MHz)	b' (MHz)	Distance to the B nucleus (Å)	s to p ratio ($\alpha^2:\beta^2$)	Percentage of total
XIII	$c_{+2}y_0$	(0,104.5,0)	0.97 ± 0.01	0.291 ± 0.007	-0.34 ± 0.02	5.94	8.7:91.3	0.3
XIV	$c_{+2}y_{\pm 1}^*$	($\pm 58.5, 70.5, 0$)	0.81 ± 0.03	-0.42 ± 0.06	-0.1757 ± 0.0004	12.98	5.2:94.8	0.4
	$c_{+1}y_{\pm 1}^*$	($\pm 58.5, 70.5, 0$)	0.81 ± 0.03	-0.42 ± 0.06	-0.1757 ± 0.0004	13.81	5.2:94.8	0.4
XV	c_0y_0	(0,70,0)	0.80 ± 0.02	0.59 ± 0.02		12.48	3.7:95.3	0.5
XVI	$c_{+1}y_{\pm 3}$	($\pm 60, 70.5, 0$)	0.55 ± 0.06	0.56 ± 0.1	-0.12 ± 0.06	6.20	2.8:97.2	0.5
	$c_{-1}y_0$	(0,0,0)	0.29 ± 0.01	-0.03 ± 0.01	0.18 ± 0.02	5.67	21.6:78.4	0.04
XVII	$c_{+2}y_{\pm 2}^*$	($\pm 60, 70.5, 0$)				7.37		

shows the total orientational dependence as measured on the k_1 site EPR line in the (11 $\bar{2}$ 0) and (0001) planes. As can be seen, the hf interaction is very anisotropic, which is the case for all sites, and the largest hf interaction is about 12 MHz. It was found that the ENDOR spectra of the k_1 and k_2 sites differ only in line intensity and close to the extreme orientations $\varphi=0^\circ$ and $\varphi=90^\circ$, as for all other orientations the EPR lines lie too close together. Close to the c axis the ENDOR spectra of the two qc sites can really be distinguished (see Fig. 4). However, in this region we have the problem that all six possible orientations of one site (which are equivalent for $\mathbf{B}\parallel\mathbf{c}$) are still present in the EPR line, leading to the complication of the ENDOR spectrum in this region as well. From a comparison of the intensities in the k_1 and k_2 spectra, the lines can be tentatively assigned to either one of the two sites. Unfortunately the lines in the outer part of the spectrum tend to broaden and disappear when turning away from the extreme orientations.

An important element in the assignment of the lines in the ^{13}C ENDOR spectrum to specific ^{13}C nuclei surrounding the B impurity is provided by the *ab initio* cluster calculations by Petrenko *et al.*²³ of the hf interactions on the sB acceptor in 3C-SiC. In this calculation, due to size problems, only nuclei up to two bond lengths away from the B atom could be taken into account. The results show that the isotropic hf interaction on the C atom next to B is 203.6 MHz. On the group of three ^{13}C atoms two bond lengths away along the direction of the B-main C bond the isotropic hf interaction was calculated to be 11.9 MHz. On all other ^{13}C atoms (one or two bond lengths away from the B atom) the isotropic hf interaction is calculated to be one order of magnitude smaller, about 0.65 MHz or less. It was proposed that the spin-density distribution is cigarlike shaped oriented along the B-main C connection line away from the B atom. With the help of this model we assigned orientational dependencies to groups of nuclei. Each group (indicated by a Roman number) contains nuclei that have roughly the same distance to the B nucleus, and that are placed cylindrically symmetrically around the line going through the B-main C connection line. The groups are divided into subgroups, sometimes con-

taining only one atom, on the basis of their distance from the line through the B nucleus and the main C nucleus.

In Tables III and IV the groups of C atoms are sorted on the basis of the value of the isotropic hf interaction. All assignments as shown in the tables will be discussed below with the help of Figs. 6–14, but first a few general remarks have to be made. Figures 6 and 7 show the k_1 and k_2 sites and their immediate surroundings. In the lower right corner the laboratory axis system and the orientation of the y and c planes, which will be discussed later, is indicated. The Roman numbers of the nuclei are connected to the numbers in Tables III and IV. Three staircases (Fig. 1) have been highlighted with respect to the others in Fig. 6. They are found back in Fig. 17(b). Figures 8–14 show the fits made for the different groups of nuclei in the (11 $\bar{2}$ 0) plane, i.e., the plane containing the c axis and in the (0001) plane. The latter plane is perpendicular to the c axis. The filled and open points represent the experimental ENDOR lines as measured for the sites for various orientations. The upper panel of the figures shows the (11 $\bar{2}$ 0) plane. Along the y axis the angle between the magnetic field and the c axis is varied in the plane containing the c axis and a projection of a B-main C bond in the plane perpendicular to the c axis from $\theta=0^\circ$ ($\mathbf{B}\parallel\mathbf{c}$) to $\theta=90^\circ$ ($\mathbf{B}\parallel\text{projection}$). The lower part of the figures shows the (0001) plane. Here the y axis represents the angle between the magnetic field and the projection of a B-main C bond in the plane perpendicular to the c axis, which is varied from $\varphi=0^\circ$ ($\mathbf{B}\parallel\text{projection}$) to $\varphi=90^\circ$ ($\mathbf{B}\perp\text{projection}$). For clarity the real ENDOR spectra are shown for the extreme orientations ($\theta=0^\circ, \varphi=0^\circ$), ($\theta=90^\circ, \varphi=0^\circ$), and ($\theta=90^\circ, \varphi=90^\circ$) as well. The orientational dependencies were also measured between $\theta=-25^\circ$ and $\theta=0^\circ$ and for $\theta=90^\circ$ to $\theta=115^\circ$. They are not shown in the figures for clarity. The lines are the fits to the points for the different groups with the parameters as can be found in Table III for the k_1 site, and in Table IV for the k_2 site. Columns one of Tables III and IV give the number of a group. These numbers can be found back in Figs. 6 and 7 for the k_1 and k_2 sites. Columns two give the position of the nucleus in the crystal

TABLE IV. The positions of the nuclei in the k_2 site in $6H$ -SiC, their tensor directions, hf interactions, distance to the B center, and coefficients α^2 , β^2 , η^2 . For the nuclei of groups II, III, and IV, with a question mark as superscript the determination of the second Euler angle is not very precise. The tensors of the groups VIII and XI are oriented toward the center of gravity of the p_z orbital on the main C (I), as for these nuclei there is a reasonable contribution from the dipole-dipole interaction to the anisotropic hf interaction. The first pair of nuclei of group XII and the second nucleus of group III have not been found in the orientational dependence. The total spin density found when summing over all nuclei is 86%. However, not all lines have been assigned. Nevertheless η^2 has been normalized to 100%. The atom positions with the same symbols as superscript can in principle be interchanged, but this would not affect the spin-density distribution appreciably.

k_2	Atom position	Euler angles (α, β, γ) in degrees	a (MHz)	b (MHz)	b' (MHz)	Distance to the B nucleus (Å)	s to p ratio ($\alpha^2:\beta^2$)	Percentage of total (η^2)
I	c_0y_0	(0,70,5,0)	114 ± 1	30 ± 1		1.887	9.7:90.3	36.0
II	$c_0y_{\pm 1}^?$	(0,70,5,0)	16.18 ± 0.06	2.93 ± 0.08	3.74 ± 0.07	4.75	13.6:86.4	3.7
	$c_{+1}y_0^?$	(0,70,5,0)	16.43 ± 0.1	2.66 ± 0.1	3.3 ± 0.1	4.75	14.9:85.1	3.4
III	c_0y_0	(0,77,5,0)	11.05 ± 0.07	2.15 ± 0.09	-0.26 ± 0.08	7.14	12.8:87.2	2.7
	$c_{+1}y_{\pm 1}$	(0,70,5,0)				7.14		
IV	$c_{+2}y_{\pm 1}^?$	($\pm 17,62,5,0$)	10.32 ± 0.07	4.6 ± 0.1	1.10 ± 0.09	7.78	6.0:94.0	5.3
	$c_0y_{\pm 2}$	($\pm 58,72,0$)	1.87 ± 0.02	-0.61 ± 0.03	0.62 ± 0.03	7.37	8.0:92.0	0.7
V	$c_{+1}y_0$	(0,65,0)	7.79 ± 0.05	1.43 ± 0.05	2.88 ± 0.08	9.43	13.4:86.6	1.8
	$c_0y_{\pm 1}$	(0,75,5,0)	3.86 ± 0.03	1.94 ± 0.03	0.60 ± 0.08	9.92	5.3:94.7	2.2
	$c_{+2}y_0$	(0,57,0)	2.03 ± 0.02	-0.20 ± 0.02	1.09 ± 0.04	9.10	22.4:87.6	0.3
	$c_{+2}y_{\pm 2}^*$	($\pm 60,75,5,0$)	3.86 ± 0.02	1.91 ± 0.01	0.60 ± 0.05	9.61	5.4:94.6	2.2
	$c_{+1}y_{\pm 2}$	($\pm 5,80,0$)	6.38 ± 0.07	2.69 ± 0.07	0.8 ± 0.1	9.93	6.3:93.7	3.1
VI	$c_{+1}y_{\pm 3}$	($\pm 60,70,5,0$)	6.43 ± 0.06	2.64 ± 0.06	0.74 ± 0.04	8.34	6.5:93.5	3.0
VII	$c_{+2}y_0^+$	(0,120,0)	2.63 ± 0.03	-0.89 ± 0.03	-0.08 ± 0.06	6.44	7.8:92.2	1.0
	$c_0y_{\pm 3}$	($\pm 55,68,0$)	1.06 ± 0.02	0.47 ± 0.03	-0.17 ± 0.04	6.44	6.0:94.0	0.5
VIII	$c_0y_{\pm 1}$	($\pm 33,85,0$)	2.08 ± 0.04	0.76 ± 0.04		1.887	7.0:93.0	0.9
	$c_{-1}y_0$	(0,37,0)	2.08 ± 0.04	0.76 ± 0.04		1.89	7.0:93.0	0.9

relative to the B nucleus. For this purpose the crystal is thought of as build up of two kinds of planes: first (0001)-like planes, which we take to contain two layers of nuclei, i.e., Si and C atoms, and which we call c double-planes ($\perp \mathbf{c}$); and second, (11 $\bar{2}$ 0)-like planes, also containing Si and C atoms, which we call y planes ($\perp \mathbf{y}$). In this way nuclei can be roughly positioned in the crystal (Figs. 6 and 7). The c_0 double plane, consisting of a Si plane and a C plane, contains the B nucleus (on a Si position) and the C carrying the main spin density (main C, number I). Going upwards or downwards parallel to the c axis leads to c_{+i} or c_{-i} double planes, respectively. The y_0 plane also contains the B nucleus (on a Si position) and the main C (I). The crystal is mirror symmetric in this plane. The $y_{\pm i}$ planes go forwards and back-

wards parallel to the plane of the paper of Figs. 6 and 7. Columns three in Tables III and IV give the orientation of the tensor in the crystal. The laboratory system is oriented with its z axis parallel to the c axis and its x axis in the (11 $\bar{2}$ 0) plane. The x axis lies parallel to the projection of a B-main C bond in the plane perpendicular to the c axis (i.e., in a y plane) and the y axis stands perpendicular to the x axis in the plane perpendicular to the c axis. Thus the direction (0, 0, 0) means that the local hf tensor lies parallel to the laboratory system. The following definition of the Euler angles is used. The first rotation α is around the z axis, the second one β is around the new y axis, and the third one γ is around the new z axis. Also the tensor orientations of the nuclei belonging to the B subsite with g_z at -70° from the c axis [which

TABLE IV. (Continued.)

k_2	Atom position	Euler angles (α, β, γ) in degrees	a (MHz)	b (MHz)	b' (MHz)	Distance to the B nucleus (\AA)	s to p ratio ($\alpha^2:\beta^2$)	Percentage of total (η^2)
IX	$c_0y_{\pm 4}$	($\pm 30, 70.5, 0$)	2.13 ± 0.02	0.67 ± 0.02		9.44	8.3:91.7	0.8
X	$c_{+1}y_{\pm 1}^{\#, +}$	(0, 70.5, 0)	1.77 ± 0.03	1.15 ± 0.04	-0.43 ± 0.04	12.08	4.2:95.8	1.3
	$c_{+2}y_{\pm 1}$	($\pm 60, 70.5, 0$)	1.77 ± 0.03	1.15 ± 0.04	-0.43 ± 0.04	11.41	4.2:95.8	1.3
XI	$c_0y_{\pm 3}^{\#}$	(0, 70.5, 0)	1.23 ± 0.02	0.40 ± 0.01		10.87	8.0:92.0	0.5
XII	$c_0y_{\pm 2}$	($\pm 76.7, 85, 0$)	~ 0.5	~ 0.2		3.61		
	$c_{-1}y_{\pm 1}$	($\pm 41.5, 135, 0$)	0.95 ± 0.02	-0.27 ± 0.03	0.89 ± 0.03	3.61	9.1:90.9	0.3
	$c_{+1}y_{\pm 1}$	($\pm 97, 29, 0$)	0.78 ± 0.03	-0.20 ± 0.03	-0.60 ± 0.04	3.61	10.0:90.0	0.2
XIII	$c_{+1}y_{\pm 2}$	($\pm 60, 70.5, 0$)	0.45 ± 0.01	0.09 ± 0.02	-0.13 ± 0.02	5.67	12.5:87.5	0.1
	$c_{-1}y_0$	(0, 0, 0)	0.1 ± 0.01	-0.05 ± 0.02		5.67	5.4:94.6	0.06

also lies in the $(11\bar{2}0)$ plane] were used to fit the $(11\bar{2}0)$ plane dependencies. The EPR line of this site overlaps with the one of the B site with g_z at 70° from the c axis for the angles close to the c axis. Columns 4, 5, and 6 give the hf tensor values a , b and b' in MHz. The last two columns will be explained in Sec. IV.

In the fitting procedure of the orientational dependence of the ^{13}C ENDOR lines, we started with the most clear lines

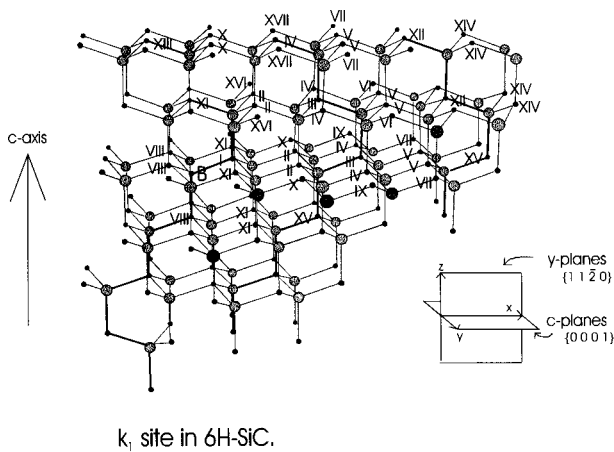


FIG. 6. A schematic representation of the crystal structure around the k_1 site in $6H\text{-SiC}$. The direction of the c axis is shown. In the right corner the orientation of the y and c planes, used in the text, has been indicated. The y_i planes, i.e., $\{11\bar{2}0\}$ planes, contain the c axis and run parallel to the surface of the paper. The c_i double planes, i.e., $\{0001\}$ planes, are the planes perpendicular to the c axis. The boron nucleus has been indicated. The Roman numbers placed near the nuclei correspond to the numbers indicating the group in Table III. The three staircases drawn with the heavy lines correspond to the ones in Fig. 17(b). The surrounding of the k site in $4H\text{-SiC}$ is exactly the same as the surrounding of this k_1 site as far as concerns the numbered nuclei.

without taking into account the position of the nuclei or the expected orientation of their hf tensor. It turned out that most of the lines were far more anisotropic than expected on the basis of a dipole-dipole interaction with the spin density on the main C. This leads to the conclusion that there is direct spin density in the p orbitals on the neighboring atoms, and that the tensors should be parallel to the bonds, i.e., $(0^\circ, 0^\circ, 0^\circ)$, $(0^\circ/180^\circ, 70.5^\circ, 0^\circ)$, $(\pm 60^\circ, 70.5^\circ, 0^\circ)$, and $(\pm 120^\circ, 70.5^\circ, 0^\circ)$. As there are some orientational dependencies with extremes that clearly deviate from these natural bond angles we concluded that in some cases linear combinations of two or more bonds directions are necessary to obtain the right angle. To obtain an idea about which tensor directions might

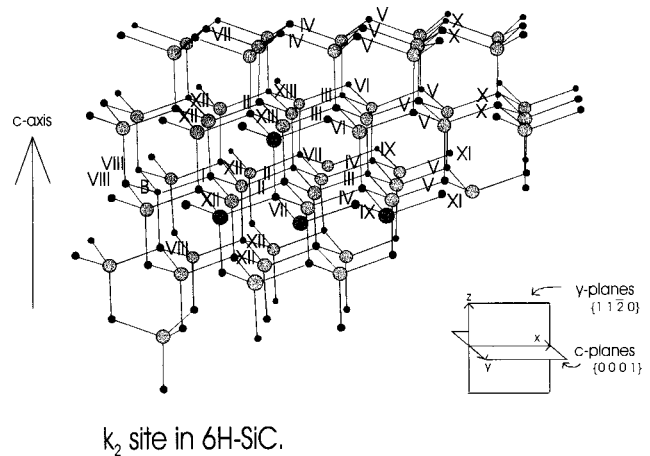


FIG. 7. A schematic representation of the crystal structure around the k_2 site in $6H\text{-SiC}$. The direction of the c axis is shown. The y_i planes contain these axes and run parallel to the surface of the paper. The c_i double planes are the planes perpendicular to the c axis. The boron nucleus has been indicated. The Roman numbers placed at the nuclei correspond to the numbers indicating the group in Table IV.

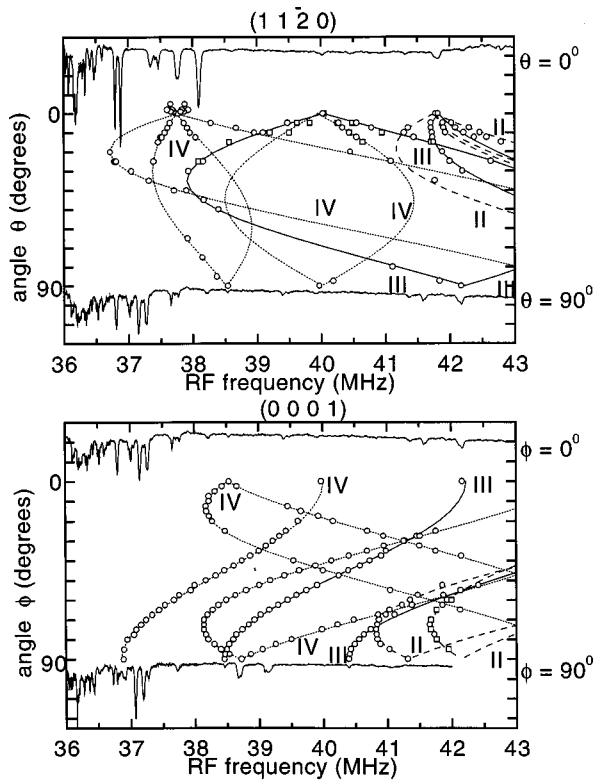


FIG. 8. The orientational dependence of the ENDOR spectrum and fits to this dependence of the k_1 site in $6H$ -SiC. The upper part of the figure shows the dependence in the $(11\bar{2}0)$ plane, and the lower part the dependence in the (0001) plane. In the $(11\bar{2}0)$ plane the angle between the magnetic field and the c axis is varied from $\mathbf{B}\parallel c$ (upper row with points) to $\mathbf{B}\perp c$ (lowest row with points). The points represent lines as measured for the different orientations. For the orientations $\mathbf{B}\parallel c$ ($\theta=0^\circ$, $\varphi=0^\circ$) and $\mathbf{B}\perp c$ ($\theta=90^\circ$, $\varphi=0^\circ$) an experimental spectrum is added for illustration. The direction $\varphi=0^\circ$ is parallel to the projection of a B-C bond in the plane perpendicular to the c axis. In the (0001) plane the direction of the magnetic field is varied from $\varphi=0^\circ$ (upper spectrum and first line with points) to $\varphi=90^\circ$ (lower spectrum and last row with points). The open points were used to fit the lines resulting in the parameters as found in Table III. This figure shows groups II, III, and IV. Group II has a dashed line, group III a full line, and group IV a dotted line. All subgroups have the same line pattern. For the nuclei of groups II.1, III.1, and IV.1 in the c_0 double plane, the crystallographic position with respect to the B nucleus is the same as for groups II.1, III.1, and IV.2 in case of the k_2 site (Fig. 12).

be reasonable for the different nuclei, we assumed that the spin density extends from nucleus to nuclei along the bonds. When starting at a nucleus the spin density tends to distribute as much as possible parallel to the direction of the B-main C connection line, and away from the B. When a nucleus can be reached by more than one bond, from another nucleus with a larger or smaller hf interaction, this leads to a tensor direction that is a linear combination, weighted roughly with the spin density on the nucleus in question, of the bond directions in question. The fits were made using the program ‘‘VISUAL EPR 12.08 Professional Edition’’ written by Professor V. Grachev.

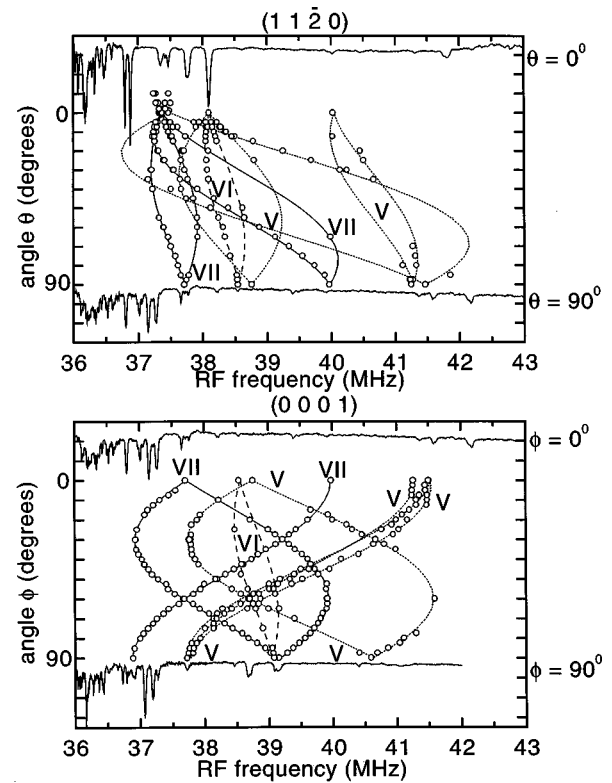


FIG. 9. The orientational dependence of the hf interaction of the ^{13}C nuclei for the k_1 site for groups V, VI, and VII. The curves of group V are dotted, those of group VI are dashed, and those of group VII are full lines. The open points were used to fit the lines resulting in the parameters as found in Table III. For the nuclei of groups V.2 and VII.1 in the c_0 double plane, the crystallographic position with respect to the B nucleus is the same as for the groups V.2 and XI.1 in the case of the k_2 site (Figs. 12 and 14). See the caption of Fig. 8 for a more general explanation of the figure.

3. Assignments of the ENDOR lines to the various groups of ^{13}C nuclei of the k_1 sB site in $6H$ -SiC

The fits of the groups II, III, IV are shown in Fig. 8. At some places in the figure the numbers of the groups have been placed next to the lines. Group II has a dashed line, group III a full line, and group IV a dotted line. All subgroups have the same line pattern. The open circles are the points with which the fits were made. The nicest orientational dependencies are found in the (0001) plane. In the $(11\bar{2}0)$ plane the outer lines broaden and disappear when turning away from the c axis. This means that for group II and subgroups III.1 and IV.1 there is no connection between the spectrum for $\mathbf{B}\parallel c$ and the (0001) plane, making the assignment slightly less certain. For the lines II.1 and IV.3, points from the orientational dependence as measured for the k site in the $4H$ -SiC crystal were also used, because there the orientational dependence was clearer. These points are given as squares. The group III nuclei are lying in the y_0 plane and thus are expected to have the same amount of spin density in bonds not lying in the plane (mirror symmetry). Their hf interaction is expected to pass through a real extreme in the $(11\bar{2}0)$ plane, and only one line is expected in the (0001) plane. The extremes are expected from crystal symmetry to be around 70° for subgroup III.1 and around 55° for sub-

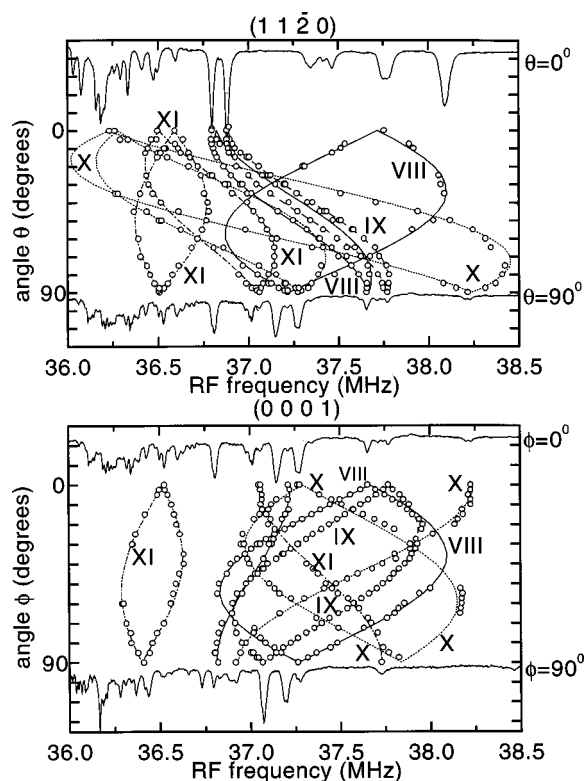


FIG. 10. The orientational dependence of the hf interaction of the ^{13}C nuclei for the k_1 site for groups VIII (full line), IX (dashed line), X (dotted line), and XI (dash-dotted line). Group VIII represents the nuclei on the other side of the B nucleus. The open points were used to fit the lines resulting in the parameters as found in Table III. For the nuclei of groups VIII, XI.1, and XI.2 (c_0 and c_{-1} double plane) and groups IX and X.2 (c_0 double plane) for the k_1 site, the crystallographic position with respect to the B nucleus is the same as for the groups VIII, and XII.1, and XII.2 and groups IX and VII.2, respectively, in the case of the k_2 site (Figs. 13 and 14). See the caption of Fig. 8 for a more general explanation of the figure.

group III.2, as is found experimentally. For the lines IV.1 and IV.2, some points have also been given for negative angles in the $(11\bar{2}0)$ plane. As far as concerns the pattern of the subgroup IV.3, the following can be said. The line at 40 MHz splits symmetrically to lower and higher frequencies when turning in the $(11\bar{2}0)$ plane; thus its extreme is expected around 45° . Consequently only the nuclei in subgroups III.2 and IV.3 (and maybe XII) are possible candidates (other nuclei are expected to have smaller hf interactions²³ or different extreme positions). Thus the inner part of this orientational dependence is assigned to subgroup IV.3 (further from the B center than subgroup III.2, and thus with smaller hf interaction) and the outer part to subgroup III.2. This assignment then dictates the orientational dependence in the (0001) plane. So the line in this plane that is already assigned to subgroup VII.1 is also assigned to subgroup IV.3. From the orientational dependencies of the group II and subgroup IV.1 nuclei, it is clear that their tensors are not lying along a bond. For these nuclei the tensor direction is a linear combination of three of the four bond directions of the nucleus. This might be expected as the nuclei are not lying in the y_0 plane, and it is easy to construct

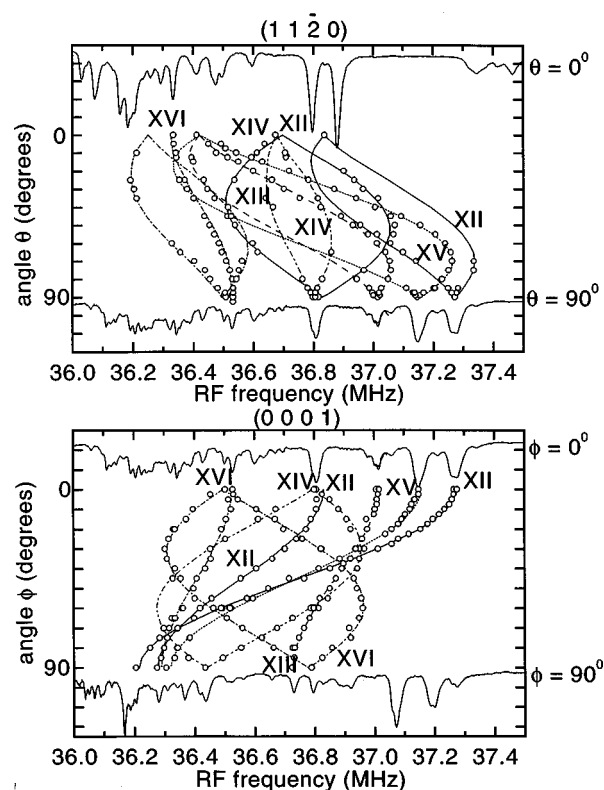


FIG. 11. The orientational dependence of the hf interaction of the ^{13}C nuclei for the k_1 site close to the Zeeman frequency of ^{13}C for groups XII (full line), XIII (dashed line), XIV (dash-double dotted line), XV (dotted line), and XVI (dash-dotted line). The open points were used to fit the lines resulting in the parameters as found in Table III. See the caption of Fig. 8 for a more general explanation of the figure.

the right linear combination making a tensor that points roughly in the direction of the center of spin density and the y_0 plane at an angle of 17° with the y_0 plane. The splitting of the line in the spectra $\varphi = 90^\circ$ and $\theta = 90^\circ$ is probably due to a slight misorientation (less than 1° is enough). One more remark can be made about this figure. The two lines assigned to group III for $\varphi = 90^\circ$ and $\theta = 90^\circ$ are only present in the spectrum of k_1 . This makes the assignment of these lines to k_1 unambiguous. The group of lines around 40.9 MHz are present in the spectra of k_1 as well as k_2 . As the intensity of the lines is the same in both spectra, we assigned these lines to k_2 .

The fits to the groups V, VI, and VII are shown in Fig. 9. The curves of group V are dotted, the ones of group VI are dashed, and the ones of group VII are full lines. The open circles show the points used for fitting. Group VI is only clear in the $(11\bar{2}0)$ plane. The orientational dependence in the (0001) plane is not clear. Without changing the pattern in the $(11\bar{2}0)$ plane, only the b' parameter can be changed, and thus only this parameter is not very certain. The orientational dependence assigned to group VI might also be assigned to the nuclei of subgroup VII.2, as the hf interaction and tensor orientations of these nuclei are expected to be roughly the same. For group VII we have a beautiful orientational dependence in both planes. Some fit points for negative angles are also shown in the $(11\bar{2}0)$ plane. The orientational dependence assigned to the nuclei of subgroup VII.2 might also be

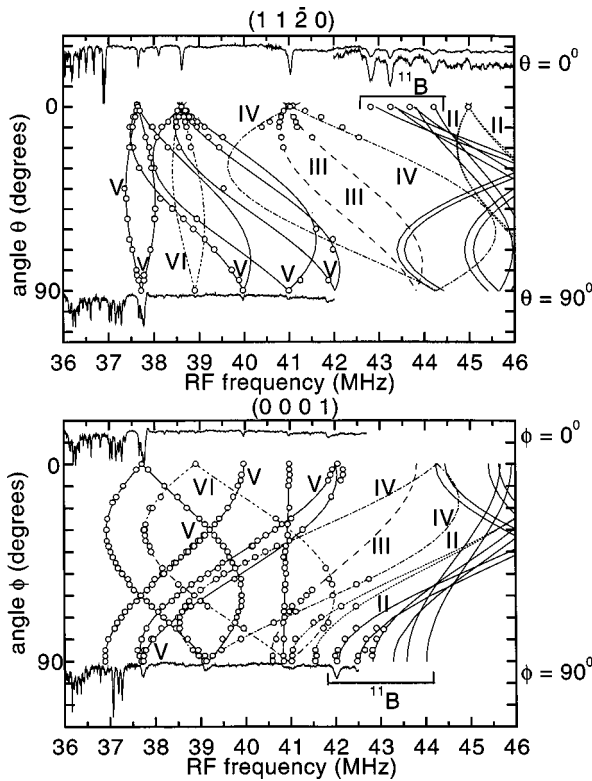


FIG. 12. The orientational dependence of the ^{11}B hf interaction of the k_1 site as well as the k_2 site, and the hf interaction of the ^{13}C nuclei of groups II, III, IV, V, and VI for the k_2 site in 6H-SiC . The lines of the ^{11}B orientational dependence are drawn as a full line, those of group II are dotted, those of group III dashed, those of group IV dash-dotted, those of group V full, and those of group VI dash-double-dotted. The ^{11}B hf lines were clearly recognizable due to their large intensity. The triplet with the largest hf interaction belongs to the k_2 site, and the one with the smaller hf interaction to the k_1 site. The open points were used to fit the lines resulting in the parameters as found in Table II for the ^{11}B lines and in Table IV for the ^{13}C lines. For the ^{13}C nuclei of groups II.1, III.1, IV.2, and V.2 in the c_0 double plane, the crystallographic position with respect to the B nucleus is the same as for groups II.1, III.1, IV.1, and V.2 in the case of the k_1 site (Figs. 8 and 9). See the caption of Fig. 8 for a more general explanation of the figure.

assigned to the nuclei of groups IX or X.2 for the same reasons as above for group VI.

Figure 10 shows the orientational dependencies of groups VIII (full line), IX (dashed line), X (dotted line), and XI (dash-dotted line). Group VIII represents the nuclei on the other side of the B nucleus. As calculated in Ref. 23, they have a very small hf interaction, though they are close to the B, suggesting that the spin-density distribution is asymmetric and directed away in one direction from the B nucleus. Their tensor is axially symmetric, and their anisotropic hf interaction is probably caused by dipole-dipole interaction, as the spin density on the B itself is negligible. Also for the nuclei of group XI the dipole-dipole interaction with the main C nucleus is still appreciable. The lines as found for group VIII.1 are clear, the arguments to ascribe the lines to group VIII.2 are mostly circumstantial, and follow from the assumption that the tensors of all three nuclei have the same principal values. The lines ascribed to group IX could also be assigned to groups VII.2 or X.2, though the latter assignment

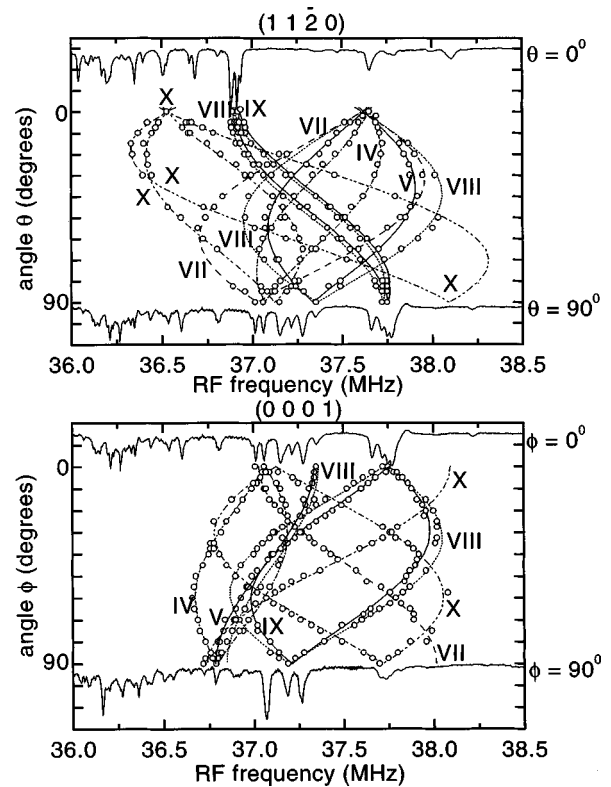


FIG. 13. The orientational dependence of the hf interaction of the ^{13}C nuclei for the k_2 site for groups IV.2 (dash-dotted line), V.3 (full line), VII.1 (dashed line), VIII (dotted line), IX (full line), and X (dash-double dotted line). Group VIII represents the nuclei on the other side of the B nucleus. The open points were used to fit the lines resulting in the parameters as found in Table IV. For the nuclei of group VIII in the c_0 double plane and the c_{-1} double plane, and group IX in the c_0 double plane of the k_2 site, the crystallographic position with respect to the B nucleus is the same as for groups VIII and IX, in the case of the k_1 site (Fig. 10). See the caption of Fig. 8 for a more general explanation of the figure.

is less probable. The line at 38.25 MHz in the spectrum for $\varphi=0^\circ$ and $\theta=90^\circ$ is assigned to k_1 as the orientational dependence of this line is much clearer for this site (compare Fig. 13). Its dependence is assigned to group X.1, the dependence of group X.2 follows by assuming that the tensors have both the same principal values. It is impossible to fit the lower part of the orientational dependence of group X.2 to the dependence starting at 37.75 MHz ($\varphi=90^\circ$ and $\theta=90^\circ$). Moreover, this line is much stronger in the spectra for k_2 (Fig. 13). The line at 37.75 MHz is thus assigned to k_2 , group X, and the dependence of group X.2 for k_1 starts just a little bit to right from this line.

Figure 11 shows the orientational dependencies close around the Zeeman frequency of ^{13}C of the lines of groups XII (full line), XIII (dashed line), XIV (dash-double dotted line), XV (dotted line), and XVI (dash-dotted line). The dependencies of groups XII, XIV, and XVI.1 are only clear in the (0001) plane, so the b' parameter found for these groups are not very certain. The orientational dependencies of the groups XIII, XV, and XVI.2 are clear in both planes. The line at 36.72 MHz for $\varphi=90^\circ$ and $\theta=90^\circ$, which is assigned to group XIII, is clearly much larger in this spectrum than in the corresponding spectrum for k_2 (Fig. 14). The orienta-

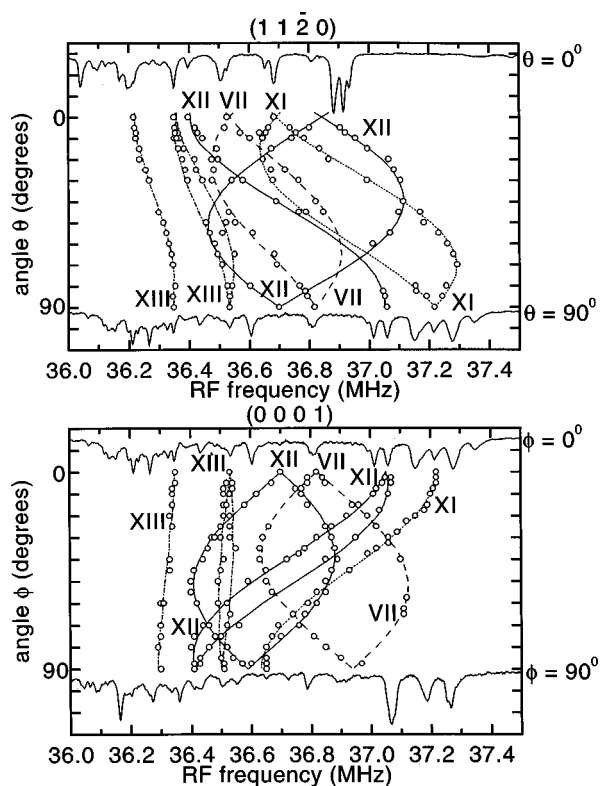


FIG. 14. The orientational dependence of the hf interaction of the ^{13}C nuclei for the k_2 site for groups VII.2 (dashed line), XI (dotted line), XII (full line), and XIII (dash-dotted line). The open points were used to fit the lines resulting in the parameters as found in Table IV. For the nuclei of groups VII.2 and XI.1 in the c_0 double plane and groups XII.1 and XII.2 in the c_0 double plane and the c_{-1} plane, the crystallographic position is the same as for groups X.2, VII.1, XI.1, and XI.2 in the case of the k_1 site (Figs. 9 and 10). See the caption of Fig. 8 for a more general explanation of the figure.

tional dependence assigned to group XIV could also be assigned to group XVII. It is also unclear whether the dependence belongs to all nuclei of group XIV or only to part of them. Some lines that are clear in the (0001) plane are not assigned because the dependence in the $(11\bar{2}0)$ plane is too unclear, and because their hf interaction is so small that they will not change the overall picture.

4. Assignments of the ENDOR lines to the various groups of ^{13}C nuclei of the k_2 sB site in 6H-SiC

Figure 12 shows the orientational dependence of the ^{11}B hf interaction of k_1 and k_2 , as well as the orientational dependence of the ^{13}C hf interaction of the groups II, III, IV, V, and VI. The lines of the ^{11}B orientational dependence are drawn as a full line, those of group II are dotted, those of group III dashed, those of group IV dash dotted, those of group V full, and those of group VI dash double dotted. The ^{11}B hf lines were clearly recognizable due to their large intensity. The intensity of the ^{11}B lines of the k_1 site is smaller as the spectrum was measured on the EPR line of the k_2 site. The triplet with the largest hf interaction belongs to the k_2 site, and the one with the smaller hf interaction to the k_1 site. The values used for the fit can be found in Table II. Of the

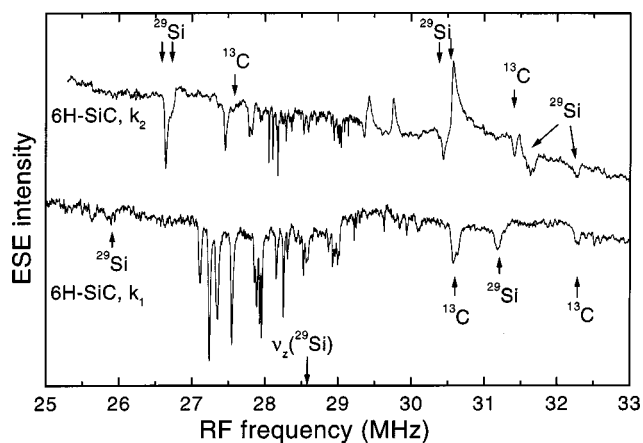


FIG. 15. The ^{29}Si ENDOR spectrum for the different sites in 6H-SiC. As for the ^{13}C ENDOR spectra, the ^{29}Si ENDOR spectrum of k_1 in 6H-SiC looks similar to the one of k in 4H-SiC. The outer Si ENDOR lines have been indicated, as have the counterparts of the outer C lines.

orientational dependence of group II, only a very small part is known. The dependence shown is based on the assumption that the tensor lies parallel to a bond, and that the hf interaction of $\mathbf{B}\parallel\mathbf{c}$ is 45 MHz and of $\mathbf{B}\parallel\mathbf{y}$ about 41 MHz. For group III the dependence is also mostly unknown, which is the reason that only one of the two dependencies has been fitted. For group IV, however, a clear dependence is visible in the (0001) plane. This assignment becomes clear if we look at the spectra for $\varphi=90^\circ$ and $\theta=90^\circ$ in Figs. 8 and 12. The line around 38.6 MHz is almost not present at all in the spectrum of k_2 (Fig. 12), whereas it is very clear in the spectrum of k_1 (Fig. 8). The line around 39 MHz is present in both spectra. Both lines exhibit exactly the same dependence, only one has a set of slightly smaller hf values than the other. The one with the smaller parameters, that is visible in the spectrum of k_1 only, was assigned to group IV of the k_1 site. Thus we attributed the dependence with the larger parameters, that is visible in both spectra, to the nuclei of group IV of the k_2 site. This suggests that the density of the electronic wave function is larger for k_2 than for k_1 at the same crystallographic site. The above assignment confirms the assignment of groups II and III, which must have a larger hf interaction than group IV. In the same way we decided that the dependence of group IV should go to the line at 41 MHz for $\mathbf{B}\parallel\mathbf{c}$. Nevertheless the value found for b' is not very certain. The orientational dependencies for group V are very nice in the (0001) plane. The line assigned to group V.1 for $\varphi=0^\circ$ and $\theta=90^\circ$ is also weakly present in the spectrum for k_1 but it is clear that this line should be assigned to k_2 as the dependence is much clearer in this case. The dependence of subgroup V.3 is discussed in the next figure, as its tensor values are much smaller. The dependence assigned to subgroups V.2 and V.4 is the same as the one assigned to group VII in the case of k_1 . We attributed these lines to k_1 as well as k_2 , because for k_1 the line in the $(11\bar{2}0)$ plane was clearer and for k_2 the line in the (0001) plane was clearer. At this crystallographic position (about 9 Å away from the B nucleus) the wave functions of the electrons connected to the k_1 or k_2 site have the same density. Closer to the B nucleus the wave function of k_2 has a larger density (compare the

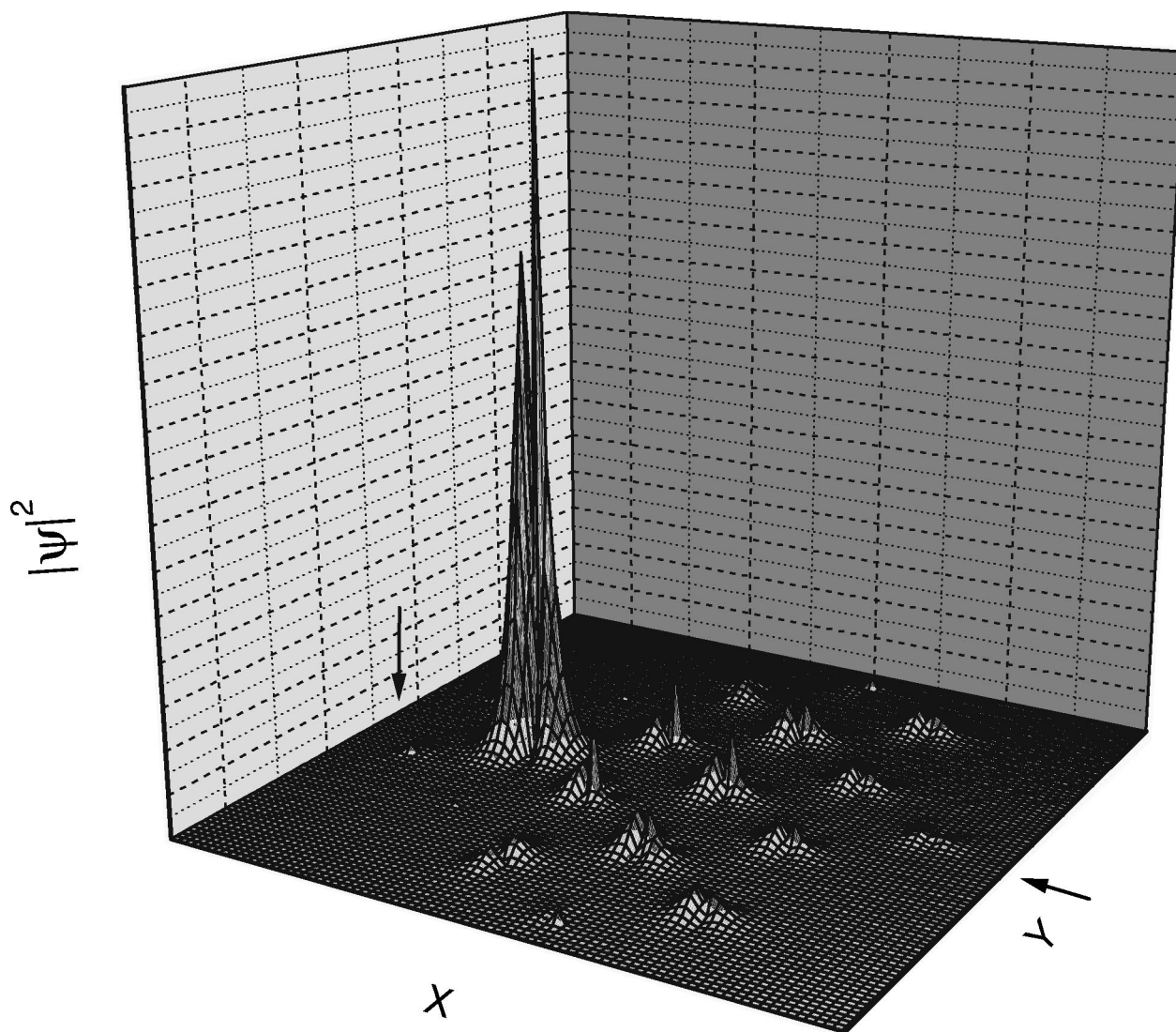


FIG. 16. The electronic wave function of the k_1 site in the c_0 double plane, which is the plane perpendicular to the c axis containing the B atom (which itself carries no spin density) and the main C atom. The intersecting line between the c_0 double plane and the y_0 plane (Fig. 17), which make an angle of 90° with each other, is indicated by two arrows. Along the z axis the value of the square of the wave function is plotted as a function of the position in the x - y plane, i.e., the position in the c_0 double plane. Only the spin density on the C atoms has been taken into account. It is seen that the spin density on the main C atom is much larger than on the other atoms. The second thing to notice is that the contribution of the $2s$ orbital to the total wave function is relatively very small, as the isotropic hf interaction is small on most nuclei.

group-IV hf tensors); further away the wave function of k_1 has a larger density. The dependence of group VI is most clear in the $(11\bar{2}0)$ plane, and is assigned to these nuclei on the grounds of its similarity with the dependence assigned to group VI in the k_1 site.

Figure 13 shows the dependencies of groups IV.2 (dash-dotted line), V.3 (full line), VII.1 (dashed line), VIII (dotted line), IX (full line) and X (dash-double-dotted line). For subgroup IV.2 the fit is very nice, as is the case for subgroups V.3 and VII.1. Group VIII contains the nuclei on the other side of B from the main C nucleus. Subgroup VIII.1 gives a good fit; the evidence for subgroup VIII.2 is somewhat more circumstantial. The dipole-dipole interaction gives a major contribution to their anisotropic hf interaction. In analogy with k_1 we would expect a second dependence of the same kind as subgroup VIII.1, as is also seen from the splitting of the line for $\mathbf{B}\parallel\mathbf{c}$. It is assigned to group IX, in analogy with

the assignment to the nuclei of group IX in k_1 . At this point it is nice to compare the group of lines around 37.75 MHz in Figs. 10 and 13 for the orientations $\varphi=0^\circ$ and $\theta=90^\circ$. It is clear from a comparison of the intensities that the two lines in the middle belong to k_2 , and that the two outer lines belong to k_1 . From the dependence of the line in the upper part of the (0001) plane, the corresponding dependence in the lower part can be found (same slope). Comparing the group of lines around 37.25 MHz for $\varphi=0^\circ$ and $\theta=90^\circ$ in Figs. 11 and 13 (and also Fig. 14), the same remark can be made. The first and third lines, when coming from higher frequencies, clearly belong to k_2 , whereas the second and fourth lines clearly belong to k_1 .

Figure 14 shows the dependencies of groups VII.2 (dashed line), XI (dotted line), XII (full line), and XIII (dash-dotted line). The dependence of group VII.2 is clear in the (0001) plane, which gives the values for a and b . In the

(11 $\bar{2}$ 0) plane the dependence is a bit less clear, and so b' is less sure. The same goes for the lines of group XII. Their anisotropic hf interaction could well be caused by the dipole-dipole interaction with the main spin density on the nearest neighbor C of the B. For group XI the dependence is somewhat clearer. For the lines assigned to group XIII, the dependence is more clear in the (11 $\bar{2}$ 0) plane than in the (0001) plane.

5. Assignments of the ENDOR lines to the various groups of ^{13}C nuclei of the k sB site in 4H-SiC

In the 4H-SiC crystal only the orientational dependence of the outer ^{13}C lines (37–42 MHz) was measured. The fits of the k_1 site in 6H-SiC can be transferred directly to the 4H-SiC k -site orientational dependence. The lines I–X are found back. As the 4H-SiC k site and the 6H-SiC k_1 site have the same surrounding for as far as we can detect with ENDOR, the same assignment to the nuclei can be used.

6. ENDOR of ^{29}Si

Figure 15 shows the ^{29}Si ENDOR spectrum for the k_1 and k_2 sites in 6H-SiC. Just as for the ^{13}C ENDOR spectra, the spectra of the k site in 4H-SiC are the same as for the k_1 site in 6H-SiC. The largest hf interaction with ^{29}Si is found in EPR ($a=10\times 10^{-4}\text{ T}\sim 28\text{ MHz}$ and $b<1\times 10^{-4}\text{ T}$). The second largest hf interaction is found from the ENDOR spectrum, and is about 5 MHz for the k_1 site and about 7 MHz for the k_2 site, though the counterpart of these lines on the low-frequency side is not found. These lines have been indicated in the figure. The counterpart of the ^{13}C lines with a large hf interaction are also indicated.

IV. DISCUSSION

The most remarkable result of our study is the assignment of lines in the ^{13}C ENDOR spectra to specific C atoms up to 11 bond lengths away from the B atom. This allows for a determination of the spatial distribution of the unpaired spin density of the sB acceptor, and in particular of an investigation of the difference in the electronic properties of the qc and hex sites in 4H-SiC and 6H-SiC. Before discussing the ^{13}C ENDOR data we first briefly review the EPR and B ENDOR results on the sB acceptor in 4H-SiC to compare them with earlier results on the sB acceptor in 6H-SiC.¹⁷

The EPR spectra indicate that the sB acceptor in 4H-SiC strongly resembles that in 6H-SiC. The principal axes of the g tensor have the same direction in the two crystals, and the principal values are almost identical. As in 6H-SiC, the g_z principal axis points along the B-main C connection line, with g_z very close to the free electron value g_e . This is typical for the situation that the spin density is mainly located in the p_z orbital on the C atom nearest to B.

The ^{13}C hf splitting observed in the EPR spectra of the sB acceptor in 4H-SiC is almost similar to that in 6H-SiC, and arises from the interaction with the C atom carrying the main spin density (main C, group I; see Figs. 6 and 7). The hf tensor is axially symmetric with the components a and b having the same sign and almost the same absolute values as in 6H-SiC. We find 2.8% s character and 32.6% p character. The fraction of p character, $32.6\%/(32.6+2.8)\%=0.92$, is

even slightly higher than the value of 0.9 found in 6H-SiC, and shows that the four orbitals of carbon in 4H-SiC have also been shifted from sp^3 hybrid orbitals towards sp^2 hybrid orbitals and one pure p orbital. With regard to the hf interaction with ^{11}B , there is no direct spin density on boron, and the isotropic hf interaction is probably caused by polarization effects. The anisotropic hf interaction b can be explained by dipole-dipole interaction with the spin density in the p_z orbital on the nearest C (group I). Using the values for the s - and p -character of 2.8% and 32.6% obtained from the hf data, we calculate $b=3.3\text{ MHz}$ using the same arguments as Matsumoto *et al.*,¹⁷ in fair agreement to the experimental value $b=2.9\text{ MHz}$. We further mention that the hf interactions of ^{11}B and ^{10}B are related very precisely by the difference in their gyromagnetic ratio. Their quadrupole interactions are related by the quadrupole moment and a spin factor. We thus conclude that there is no measurable isotope effect on the electronic properties of the sB acceptor. Also, the quadrupole splitting for ^{11}B is almost identical in 4H-SiC and 6H-SiC. Hoffstaetter *et al.*²⁸ found that, also for the sB acceptor in 3C-SiC, there is no isotope effect.

As we mentioned, the analysis of the ^{13}C ENDOR spectra allows for a determination of the spin-density distribution on the remote ^{13}C nuclei around the sB center. As shown in Sec. III, this distribution is not spherically symmetric but is highly anisotropic and directed from B to the main C and beyond (Figs. 6 and 7). This finding is in striking agreement with theoretical predictions of Petrenko *et al.*²³ These authors performed semiempirical, quantum-chemical modified neglect of differential overlap (MNDO) calculations on a $\text{B}_{\text{Si}}\text{Si}_{42}\text{C}_{44}\text{H}_{76}$ cluster in cubic SiC and obtained the hf interaction on the C and Si atoms. For the main C atom (group I) they predict $a=203.6\text{ MHz}$ and $b=75.1\text{ MHz}$ compared with our findings of $a=114.24\text{ MHz}$ and $b=30.24\text{ MHz}$. For the group-II C atoms, they calculate $a=11.91\text{ MHz}$, $b=2.09\text{ MHz}$, and $b'=0.32\text{ MHz}$, which compare remarkably well with our values found for the ^{13}C nuclei connected to sites k_1 and k_2 in 6H-SiC and site k in 4H-SiC. Unfortunately the number of C atoms in the cluster calculation is much smaller than the number of assigned ^{13}C atoms in the ENDOR analysis. For this reason we can only compare the hf data of C atoms belonging to groups VIII, XI, XV, and XVI with the theoretical values. All these groups of C atoms have a calculated isotropic hf interaction that is smaller than 0.6 MHz, and an anisotropic hf interaction smaller than 0.8 MHz. These values are an order of magnitude smaller than the hf interaction with the group-II ^{13}C nuclei. Inspection of Figs. 6 and 7 thus leads to the conclusion that the spin density is not spherical around B but rather directed along the B-main C bond and beyond. All the other assigned hf interactions agree with this general behavior.

To translate the observed and assigned ^{13}C hf interactions into electron densities, we take the point of view that the wave function of the sB acceptor consists mostly of $2s$ and $2p$ orbitals of the C atoms. This is based on the idea that the atomic $2s$ and $2p$ C energy levels lie lower than the $3s$ and $3p$ Si levels, and that consequently the bonding linear combination of atomic orbitals-molecular orbital (LCAO-MO), which should reflect the properties of the valence band, consists mostly of $2s$ - $2p$ C orbitals, i.e., the hole is expected to

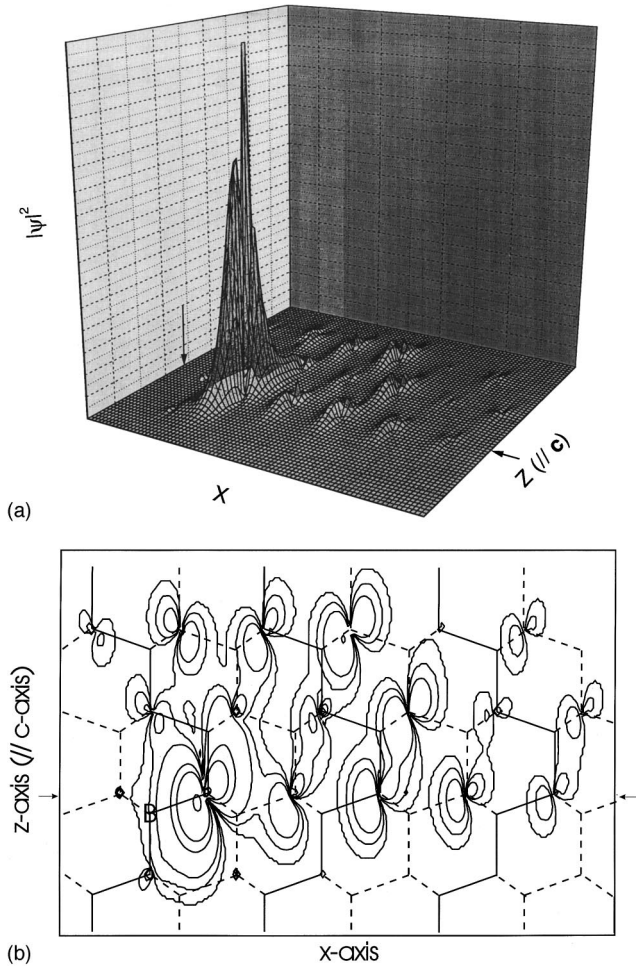


FIG. 17. (a) The electronic wave function of the k_1 site in the y_0 plane, containing the B atom and the main C atom. The intersecting line between the c_0 double plane (Fig. 16) and the y_0 plane, which make an angle of 90° with each other, is indicated by two arrows. The position of the main C atom is clearly recognizable, as in Fig. 16, by the large peak at that position. (b) The value of the square of the wave function is shown as a function of the position in the xz ($=y_0$) plane using a contour plot. Each line indicates a certain height and the larger the amount of lines the higher is the peak. The B nuclear position is indicated (left under). The position of the main C atom can be recognized from the large number of contour lines. The full lines indicate the c axes located in the y_0 plane, and the dotted lines indicate the projection of the two c axes located in the $y_{\pm 1}$ planes into the y_0 plane. It is clear that the spin density is very anisotropic. The distribution points away from the B atom into one direction only along the B-C connection line, making an angle of 70° to the c axis. The nuclei on the other side of the B atom carry an almost negligible amount of spin density. Comparing this wave function to the wave function of the electron at a k_2 position (Fig. 18), it is seen that the electron located at a k_1 position in the crystal is slightly more delocalized.

be located mostly on the C atoms, as was already mentioned in Sec. I.²² To model the wave function of the unpaired electron bound to the sB center, we consider the wave function as a LCAO-MO centered on C atoms near the defect, i.e.,

$$\Psi = \sum \eta_i \psi_i \quad \text{with} \quad \sum \eta_i^2 = 1. \quad (2)$$

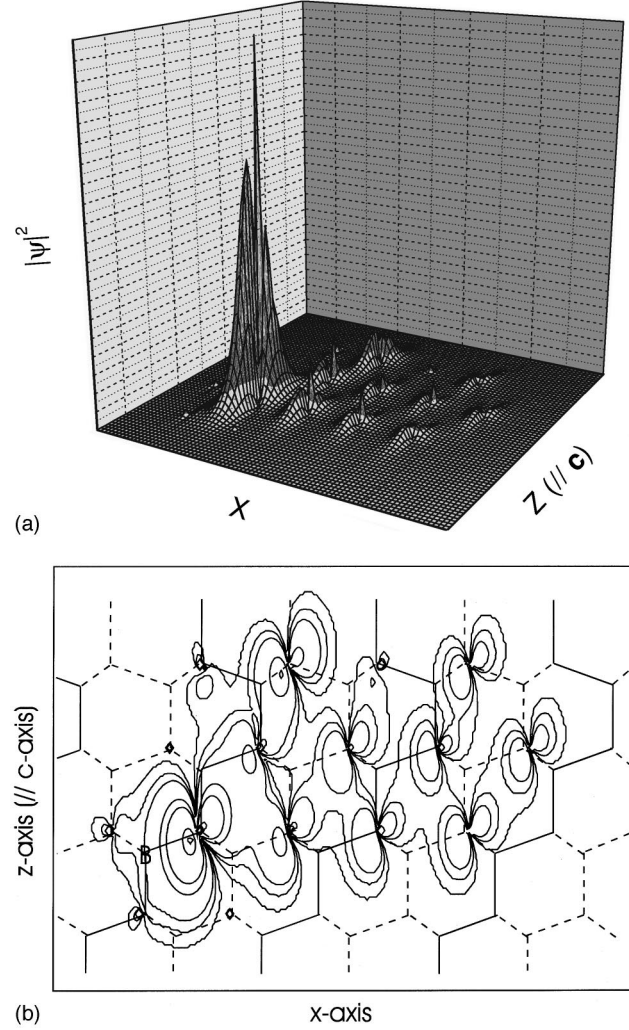


FIG. 18. (a) The electronic wave function of the k_2 site in the y_0 plane, containing the B atom and the main C atom. The position of the main C atom is clearly recognizable, as in Fig. 17, by the large peak at that position. (b) The value of the square of the wave function is shown as a function of the position in the xz ($=y_0$) plane using a contour plot. It can be seen that the wave function at this site is slightly more localized than at a k_1 position (Fig. 17).

At each C atom, we approximate the atomic function as a $2s$ - $2p$ hybrid orbital

$$\psi_i = \alpha_i (\psi_{2s})_i + \beta_i (\psi_{2p})_i \quad \text{with} \quad \alpha_i^2 + \beta_i^2 = 1. \quad (3)$$

Here the $2p$ orbital is oriented along one of the four possible Si-C connection lines. For some C atoms, however, we have to take a linear combination of $2p$ orbitals to obtain the experimentally found direction for the tensor. The relation between the isotropic and anisotropic hf interactions and the spin densities is obtained using the table of Morton and Preston.²⁹ The ratio of the isotropic and the anisotropic hf interaction is determined by $\alpha^2:\beta^2$. Taking the sum of the spin densities of all C atoms for k_1 , we find values of 105%, and, for k_2 , 86%. It is not surprising that these values are not equal to 100%. First, not all ^{13}C hf lines were fitted and assigned; second, a small amount of spin density is located on the Si atoms; and third, no polarization effects were taken into account. We normalize the total amount of spin density

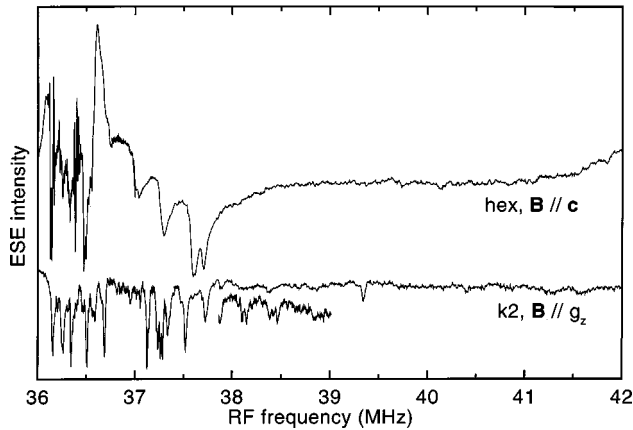


FIG. 19. The ^{13}C ENDOR spectrum of the hex site for $\mathbf{B}\parallel g_z$ (c axis) and of the qc sites for $\mathbf{B}\parallel g_z$. In this orientation the difference between the three qc sites (k , k_1 , and k_2) is only in the intensity of the lines. It is seen that though the qc site ENDOR spectrum still contains some lines above 38 MHz, the hex one does not. Moreover, it is seen that the outer hex-site ENDOR lines are very broad.

that is found to 100% by dividing the percentage of spin density for each atom by the total percentage of spin density that is found. This gives the percentage of spin density per atom, η^2 . In columns 9 and 10 of Tables III and IV, we give the values for α^2 , β^2 , and η^2 for the different ^{13}C . By using formulas (2) and (3), Tables III and IV, and the Roothaan-Hartree-Fock wave functions,³⁰ we can calculate the square of the total wave function of the electron at any point in space. In this we have assumed that the spin density is the same as the electron density, even though the center of the spin density is not the same as the center of charge density (\mathbf{B} is neutral).

To visualize the delocalization of the electronic wave function connected to the k_1 site, we show in Fig. 16 its spin density at C atoms in the c_0 double plane. Here the density on the main C atom dominates, but there is an appreciable delocalization beyond this carbon atom away from B. In Fig. 17 we again show the spin density of k_1 but now in the y_0 plane, that is, the plane perpendicular to the c_0 double plane and containing the c axis. Figure 17(a) shows the wave function in a three-dimensional representation, and Fig. 17(b) shows the wave function in the form of a contour plot. To make an illustrative figure, the C atoms in the $y_{\pm 1}$ planes have been projected onto this y_0 plane. The crystal can be regarded as a collection of staircases along the c axis (Fig. 1). The staircase on which the B and the main C are situated is located in the y_0 plane, and is indicated as a full line in Fig. 17(b) (Fig. 6). The next staircases are located in the y_+ and y_- planes, are projected onto y_0 , and are indicated by a dotted line. The next staircase along the x direction is again located in the y_0 plane. It is seen that the electron density is distributed in an ellipsoidal shape with the main symmetry axis making an angle of 70° with the c axis, i.e., along the direction of the B-main C line. Figures 18(a) and 18(b) show the electronic wave function connected to the k_2 site in the y_0 plane. Figures 17 and 18 can be compared, as they show the same plane on the same scale, and we can see that the electronic wave function of the k_1 site is slightly more delocalized than that of the k_2 site.

The fact that all three sB centers in $6H$ -SiC seem to have different localizations of the spin density (for the hex site, see the discussion below) and thus different ionization energies supports the results of Evwaraye *et al.*,²⁰ who found three different levels for the sB acceptor at $E_h = E_v + 0.27$ eV, $E_{k_1} = E_v + 0.31$ eV, and $E_{k_2} = E_v + 0.38$ eV. It seems probable that the k_2 -related energy level, which lies much lower than the hex- and k_1 -related ones, leads partly to self-compensation in the crystal. This might be the basis for the explanation of the change in electrical characteristics that is found when going from $4H$ -SiC to $6H$ -SiC. Another important result of our findings is a proposed reassignment of the ionization energy levels found for the sAl and sGa acceptors. Until now it was always supposed that the k_1 and k_2 sites were paired,²¹ having the larger ionization energy, whereas the hex site had a smaller ionization energy. We instead propose that the smaller ionization energy should be assigned to the hex and k_1 sites, with the k_2 site having the larger energy. This is in agreement with the ODMR results of Lee *et al.*¹⁴ and Maier *et al.*,¹⁰ who found that for the sAl acceptor in $4H$ -SiC two lines are found around $g \sim 2.3$, whereas in $6H$ -SiC a third line is found at a much smaller g value. As these centers obey effective-mass theory, this tells us that the third line belongs to a much deeper center. As explained, the k site in $4H$ -SiC is related to the k_1 site in $6H$ -SiC, leading to the conclusion that the third line belongs to the k_2 site, in agreement with our results.

The question arises whether the anisotropic distribution of the electronic wave function on the remote ^{13}C nuclei as revealed by the ^{13}C ENDOR data can be rationalized on the basis of effective-mass theory (EMT). As mentioned in Sec. I, sGa and sAl, in contrast to sB, show a highly anisotropic g tensor in agreement with the calculated g anisotropy of the valence-band hole. In the case of the sB acceptor the orbital angular momentum is quenched, and one would not expect to see band-structure properties reflected in the properties of the hole attached to the sB acceptor. Nevertheless we observe that the electronic wave function of the qc sB acceptor perpendicular to the c axis extends considerably further than parallel to the c axis, in agreement with the anisotropy of the hole mass ($m_{\text{hole}}^{\parallel} = 1.67m_e$ and $m_{\text{hole}}^{\perp} = 0.62m_e$).³¹ Here we remark that the anisotropy in the perpendicular plane is averaged out at higher temperatures, where it is known that the B-main C bond starts to jump between the three possible directions of this bond. The cylindrically symmetric spin density so obtained spreads out further in the perpendicular plane than along the c axis.

In the case of the hex-site sB acceptor, it is less clear whether the same picture applies. Here again the main spin density is located in the dangling p_z orbital on the nearest-neighbor C. This time, however, the B-main C connection line is parallel to the c axis. So the central core of the spin-density distribution is the same as for the qc sites. If the spin-density distribution on the remote ^{13}C would exhibit a shape similar to that for the qc sites, it would extend as an ellipsoid with its main axis parallel to the c axis. However, if EMT theory would apply, one would expect the spin density on the remote ^{13}C to extend in the perpendicular plane. Figure 19 shows the ENDOR spectrum as measured on the hex-site EPR line for $\mathbf{B}\parallel c$. Comparison with the spectra of the qc sites for the $\mathbf{B}\parallel$ B-main C connection line shows that the hex-

site ENDOR lines exhibit a smaller maximum hf interaction, and that the lines cluster around the Zeeman frequency. Moreover, the qc sites have ENDOR lines above 38 MHz for all orientations, whereas for the hex site this is not the case. A possible explanation for this is that the spin density on the remote ^{13}C is distributed mainly in the plane perpendicular to the c axis. In this case the orientational dependence of the ENDOR lines would look completely different from the dependence of the qc sites, and would cluster more around the free ^{13}C Zeeman frequency. Moreover, owing to the cylindrical symmetry of the hex site around the c axis, more ^{13}C nuclei are involved in the ENDOR spectrum than for the qc sites, thus explaining the broad ENDOR lines in the case of the hex site. We conclude that the ^{13}C ENDOR spectrum of the hex site is consistent with a distribution of the electron density on the remote ^{13}C perpendicular to the c axis, as one would expect on the basis of the anisotropy of the effective mass. So, when comparing the qc sites with the hex site, we see that the distribution of the spin density on the remote ^{13}C depends on the orientation of the core of the electronic wave function and the anisotropy of the effective mass in the crystal.

With regard to the Si ENDOR spectrum, we found that the k site in $4H$ -SiC is the same as the k_1 site in $6H$ -SiC, and that the k_2 site is different. From Fukumoto,²² it is expected that the amount of spin density on the Si atoms is small. The largest hf interactions found for Si are $a \sim 28$ MHz and $b < 2.8$ MHz. This leads to an s -spin density of 0.6% on each of the three Si is connected to the main C. The next largest hf interaction for the Si nuclei after the one found in EPR is about 6 MHz, which corresponds to 0.1% of the s -spin density or 2% of the p -spin density. So most probably the total amount of spin density on the Si atoms is much less than 10%, justifying our use of only the C spin density in calculating the electron wave-function distribution.

As a last remark it should be mentioned that we found no indication that the principal values of the g and hf tensors change with temperature between 1.5 and 4.2 K, in contrast to what is reported in Ref. 32. A possible explanation for this might be that another center was measured in these experiments at 1.5 K.

V. CONCLUSION

We have been able to determine the spatial distribution of the electronic wave function of the shallow boron acceptor at the quasicubic sites in $4H$ -SiC and $6H$ -SiC up to 14 Å away from the B atom. It is found that the delocalization of this wave function is very anisotropic, and that it agrees very

well with the theoretical predictions based on semi-empirical MNDO calculations on a $\text{B}_{\text{Si}}\text{Si}_{42}\text{C}_{44}\text{H}_{76}$ cluster by Petrenko *et al.*²³ Although the EPR spectrum of the sB acceptor shows that the orbital angular momentum is quenched, $g \sim 2$, in contrast to the sAl and sGa acceptors, the spatial distribution of the electronic wave function for the remote nuclei can be rationalized in terms of the anisotropy of the hole effective mass. Moreover, it is found that the k_2 -site electronic wave function is slightly more localized than the k_1 -site wave function, suggesting that the k_2 site has a larger ionization energy than the k_1 site. The measurements also suggest that for the hexagonal site the spatial distribution on the remote ^{13}C nuclei is different from that at the quasicubic sites, in that it extends isotropically in the plane perpendicular to the c axis. So, when comparing the qc sites with the hex site, we conclude that the distribution of the spin density on the remote ^{13}C is determined by two factors. The first one is the orientation of the core of the electronic wave function, parallel to c for the hex site and at 70° to the c axis for the qc sites. The second one is the anisotropy of the effective mass in the crystal, which leads to a suppression of the distribution along the c axis. Our results support the assignment of ionization energies $E_h = E_v + 0.27$ eV, $E_{k_1} = E_v + 0.31$ eV, and $E_{k_2} = E_v + 0.38$ eV by Evwaraye *et al.*²⁰ Thus we propose that the addition of the k_2 site, which leads to an (additional) deeper level and to partial self-compensation in $6H$ -SiC, might be the basis for an explanation of the change in electrical characteristics found when going from $4H$ -SiC to $6H$ -SiC. Another important result of our findings is a proposed reassignment of the two ionization energy levels found for the sAl and sGa acceptors. Instead of relating the k_1 and k_2 sites²¹ to the deeper level, and assigning the smaller of the two ionization energies to the hex site, we propose to relate the hex and k_1 sites to the shallower level, and to assign the k_2 site to the deeper level. This is in agreement with the ODMR results of Lee *et al.*¹⁴ and Maier *et al.*¹⁰ The results show the potential of EPR and ENDOR spectroscopy at 95 GHz for elucidating the electronic structure of the sB acceptor centers in SiC.

ACKNOWLEDGMENTS

This work forms part of the research program of the ‘‘Stichting voor Fundamenteel Onderzoek der Materie’’ (FOM) with financial support from the ‘‘Nederlandse Organisatie voor Wetenschappelijk Onderzoek’’ (NWO). P.G.B. acknowledges support by NWO under Grant No. 047.005.12.96.

¹G. Feher, Phys. Rev. **114**, 1219 (1959).

²E. B. Hale and R. L. Mieher, Phys. Rev. **184**, 739 (1969).

³E. B. Hale and R. L. Mieher, Phys. Rev. **184**, 751 (1969).

⁴G. Feher, J. C. Hensel, and E. A. Gere, Phys. Rev. Lett. **5**, 309 (1960).

⁵G. Pensl and R. Helbig, *Festkoerperprobleme: Advances in Solid State Physics* (Vieweg, Braunschweig, 1990), Vol. 30, p. 133.

⁶M. M. Anikin, A. A. Lebedev, A. L. Syrkin, and A. V. Suvorov,

Fiz. Tekh. Poluprovod. **19**, 114 (1985); [Sov. Phys. Semicond. **19**, 69 (1985)].

⁷W. Suttrop, G. Pensl, and P. Laning, Appl. Phys. A: Solids Surf. **51**, 231 (1990).

⁸H. H. Woodbury and G. W. Ludwig, Phys. Rev. **124**, 1083 (1961).

⁹A. G. Zubatov, I. M. Zaritskii, S. N. Lukin, E. N. Mokhov, and V. G. Stepanov, Fiz. Tekh. Tela (Leningrad) **27**, 322 (1985); [Sov.

- Phys. Solid State **27**, 197 (1985)].
- ¹⁰K. Maier, J. Schneider, W. Wilkening, S. Leibenzeder, and R. Stein, Mater. Sci. Eng., B **11**, 27 (1992).
- ¹¹N. P. Baran, V. Ya. Bratus, A. A. Bugai, V. S. Vikhnin, A. A. Klimov, V. M. Maksimenko, T. L. Petrenko, and V. V. Romanenko, Phys. Solid State **35**, 1544 (1993).
- ¹²P. G. Baranov, I. V. Ilyin, and E. N. Mokhov, Solid State Commun. **100**, 371 (1996).
- ¹³P. G. Baranov, Defect Diffus. Forum **148–149**, 129 (1997).
- ¹⁴K. M. Lee, Le Si Dang, G. D. Watkins, and W. J. Choyke, Phys. Rev. Lett. **45**, 390 (1980).
- ¹⁵P. G. Baranov, V. A. Vetrov, N. G. Romanov, and V. I. Sokolov, Fiz. Tekh. Tela. (Leningrad) **27**, 3459 (1985); [Sov. Phys. Solid State **27**, 2085 (1985)].
- ¹⁶P. G. Baranov and N. G. Romanov, Appl. Magn. Reson. **2**, 361 (1991).
- ¹⁷T. Matsumoto, O. G. Poluektov, J. Schmidt, E. N. Mokhov, and P. G. Baranov, Phys. Rev. B **55**, 2219 (1997).
- ¹⁸T. L. Petrenko, V. V. Teslenko, and E. N. Mokhov, Fiz. Tekh. Peluprovodn. **26**, 1556 (1992); [Sov. Phys. Semicond. **26**, 874 (1992)].
- ¹⁹R. Muller, M. Feege, S. Greulich-Weber, and J.-M. Spaeth, Semicond. Sci. Technol. **8**, 1377 (1993).
- ²⁰A. O. Evwaraye, S. R. Smith, W. C. Mitchel, H. McD. Hobgood, G. Augustine, and V. Balakrishna, Mater. Sci. Forum **258–263**, 691 (1997).
- ²¹M. Ikeda, H. Matsunami, and T. Tanaka, J. Lumin. **20**, 111 (1979).
- ²²A. Fukumoto, Phys. Status Solidi B **202**, 125 (1997).
- ²³T. L. Petrenko, V. V. Teslenko, A. A. Bugai, V. D. Khavryutchenko, and A. A. Klimov, Semicond. Sci. Technol. **11**, 1276 (1996).
- ²⁴Yu. A. Vodakov, E. N. Mokhov, M. G. Ramm, and A. D. Roenkov, Krist. Tech. **5**, 729 (1979).
- ²⁵R. T. Weber, J. A. J. M. Disselhorst, L. J. Prevo, J. Schmidt, and W. Th. Wenckebach, J. Magn. Reson. **81**, 129 (1989).
- ²⁶J. A. J. M. Disselhorst, H. van der Meer, O. G. Poluektov, and J. Schmidt, J. Magn. Reson. **115**, 183 (1995).
- ²⁷W. B. Mims, in *Electron Paramagnetic Resonance*, edited by S. Geschwind (Plenum, New York, 1972).
- ²⁸A. Hoffstaetter, B. K. Meyer, A. Scharmann, P. G. Baranov, I. V. Ilyin, and E. N. Mokhov, Mater. Sci. Forum **264–268**, 595 (1998).
- ²⁹J. R. Morton and K. F. Preston, J. Magn. Reson. **30**, 377 (1978).
- ³⁰E. Clementi and C. Roetti, At. Data Nucl. Data Tables **14**, 185 (1974).
- ³¹W. R. L. Lambrecht, S. Limpijumngong, S. N. Rashkeev, and B. Segall, Phys. Status Solidi B **202**, 5 (1997).
- ³²S. Greulich-Weber, F. Feege, K. N. Kalabukhova, S. N. Lukin, J. M. Spaeth, and F. J. Adrian, Semicond. Sci. Technol. **13**, 59 (1998).